[American Journal of Science, Vol. 318, November, 2018, P. 921–948, DOI 10.2475/09.2018.03]

REVIEW OF THE CURRENT STATUS AND CHALLENGES FOR A HOLISTIC PROCESS-BASED DESCRIPTION OF MASS TRANSPORT AND MINERAL REACTIVITY IN POROUS MEDIA

SERGEY V. CHURAKOV*,**,† and NIKOLAOS I. PRASIANAKIS**

ABSTRACT. Reactivity of minerals is controlled by chemical processes at mineral-fluid interfaces acting at different time- and length scales. Various modeling approaches are available to characterize scale-specific aspects of mineral-fluid interface chemistry. Most fundamental aspects of mineral reactivity are provided by atomic scale simulations. Several attempts have been made to interpret macroscopic observation based on atomic scale simulations alone. Many of them have failed however, because of neglecting the pore scale transport phenomena. Pore scale simulation, provide an elegant way to link idealized nanometer scale atomistic description of mineral reactivity with structural and compositional heterogeneities of natural systems. The main challenges are the spatial and temporal coupling of physical models and the upscaling of transport parameters for the macroscopic interpretation of the system behavior. This paper summarizes the current molecular-scale knowledge on mineral-fluid interface chemistry, obtained from complementary coarse-grain simulation approaches. Using the most recent developments in this field, we highlight the complexity and challenges of the pore-scale modeling and suggest a roadmap for the process-based description of mineral dissolution/precipitation across different scales.

Key words: Reactive transport, upscaling, Lattice Boltzmann, molecular dynamics, Monte Carlo, mineral-fluid interface, Electric Double Layer, dissolution-precipitation, porosity-permeability-diffusivity

INTRODUCTION

Chemical weathering and hydrothermal mineralization are prominent examples of a strong geochemical coupling between mineral reactivity and mass transport in porous media. The re-construction of mineral and rock alteration processes often relies on field-scale multicomponent reactive transport simulations. In this approach, the differential equations describing advective and diffusive transport of chemical species in heterogeneous porous media are coupled to algorithms that yield the equilibrium- or kinetically controlled chemical speciation (Steefel and others, 2015a). Such a system of equations is solved numerically on a discrete spatial grid. The finest element of this discretization is called the *Representative Element Volume* (REV), within which the material properties, the chemical composition, and the transport parameters are homogenized. Mass fluxes in chemically inert systems are well understood. The solute transport in such systems is fully controlled by chemical and hydraulic gradients via functional relationships relating porosity ($\varepsilon[-]$), permeability ($\kappa_s[L^2]$), and diffusivity $D_e[L^2t^{-1}]$. These relations may apply to individual mineral phases or even to an entire geological formation and would remain invariant during the simulation. The interplay between porosity and permeability/ diffusivity is often modeled by using empirical power laws such as Archie's and Kozeny-Carman equations or their modifications (Revil and Cathles, 1999; Xu and Yu, 2008; Van Loon and Mibus, 2015) (eqs. 1, 2):

$$D_e = D_0 \varepsilon^m \tag{1}$$

* University of Bern, Institute of Geological Sciences, CH-3012 Bern, Switzerland
** Laboratory for Waste Management, Nuclear Energy and Safety Department, Paul Scherrer Institut, CH-5232 Villigen, Switzerland
† Corresponding author: sergey.churakov@psi.ch

$$\kappa_s = \kappa_0 \left(\frac{\varepsilon}{\varepsilon_0} \right)^{\gamma} \tag{2}$$

where D_0 is the pore diffusion coefficient of species in solution, κ_0 is the reference permeability of the medium, and m, γ are empirical parameters. Even though such equations are not likely to reflect the detailed transport mechanisms, their parameters can be fitted to the experimental data and then directly applied to large-scale solute transport simulations.

As recognized by the scientific community (Xie and others, 2015), the aforementioned approach has several limitations. The level of complexity increases when chemistry starts to play a role. Heterogeneous (dissolution or precipitation) reactions alter the internal structure and porosity of the media, and thus, inevitably modify the initial transport parameters. The couplings between dissolution or precipitation reactions and solute transport can have a strong non-linear feedback on mass fluxes and onto the time scale of the geochemical alteration process. For instance, preferential transport pathways may become impermeable in the event of precipitation, even if the total average porosity within an REV remains high (Poonoosamy and others, 2015; Poonoosamy and others, 2016). Alternatively, the reaction-transport coupling may lead to the formation of preferential dissolution pathways, thus facilitating the mass transport in a consolidated low-porosity formation (Putnis and Mezger, 2004; Ruiz-Agudo and others, 2014; Putnis, 2015). Equations 1 and 2 may have a limited range of applicability when precipitation and dissolution reactions play a prominent role, and the concept of REV breaks down. For example, in complex simulations, macroscopic reactive transport codes do not converge to a consistent result upon refining the grid resolution at the location of strong chemical gradients (Marty and others, 2009).

Kinetics of heterogeneous chemical reactions (surface reactivity R[M t^{-1}]) in geochemical systems is often described by the affinity-based closed-form equations (Brantley and others, 2007):

$$R = -S \sum_j \rho_j k_j \prod_i a_{j,i}^{v_{j,i}} (1 - \Omega^{p_i})^{q_i} \tag{3}$$

$$k_j = A_j e^{\frac{-E_j^a}{k_B T}} \tag{4}$$

The first term S represents the reactive surface area of a mineral [L^2]. The sum accounts for the possible contributions of different reaction mechanisms. The rate constants, k_j, for the individual reactions are described by an Arrhenius type equation, (eq. 4), where A_J is the pre-exponential factor describing the collision frequency [t^{-1}], E_j^a is the (effective) activation energy, T is the temperature [K], and k_B is the Boltzmann constant. The parameter ρ_j, defines the density of reactive surface sites [M L^{-2}]. The activity product raised to the power of the stoichiometric coefficients, $\prod_i a_{j,i}^{v_{j,i}}$, accounts for the number of species involved in the rate controlling reaction steps (reaction order). The last term describes the deviation of the system composition from equilibrium, that is, the thermodynamic affinity, and indicates the net direction of the kinetic process. Ω is the saturation index that equals to unity at equilibrium, whereupon the kinetic rate R becomes zero. Equation 3 is routinely applied to both mineral dissolution ($\Omega < 1$) and growth ($\Omega > 1$) processes.

The description of kinetics with equation 3 is popular because of its simplicity and a direct relation (via the affinity term) to the partial thermodynamic equilibrium state. At a first glance, the other parameters can be easily determined from experiments. The difficulties, however, become evident when the temporal and the spatial evolution of

the system are considered. Firstly, the numerical value of the surface area depends on the measurement technique (for example, scale dependent), and is not expected to remain constant during reactive processes. Depending on the flow and chemical conditions, the evolution of surface area within the same REV can follow different paths (Prasianakis and others, 2018). Secondly, the reactive surface site density depends on the type of exposed crystal faces and on the surface morphology, which may all undergo stochastic variations with time (Fischer and others, 2014). Thirdly, the site reactivity, that is the product of the Arrhenius exponent and the pre-exponential factor, may also depend on the chemical composition of the system in the vicinity of the interface. The most typical examples of such dependencies may be the passivation of reactive surface sites or, in contrary, catalytic effects induced by adsorbed complexes [for example, (Vinson and others, 2007)]. The inhibiting effects, for example, may appear at a well-defined concentration threshold and depend on the distance of the system from thermodynamic equilibrium in a strongly nonlinear way (Teng, 2004; Xu and others, 2012). Recent studies have shown that even very low concentrations of Mg^{2+}, SO_4^{2-} and other ions (for example, Zn, Cd) may have a substantial impact on the surface reactivity of calcite (Mucci and Morse, 1983; Lea and others, 2001; Freij and others, 2005; Arvidson and others, 2006; Vinson and others, 2007). This is usually interpreted as relatively strong adsorption of inhibitors on surface sites, which makes them less accessible for other molecules. Finally, a comprehensive compilation of mineral reactivity data shows that the reaction rates and rate constants in equation 3, evaluated using different widely accepted experimental protocols, may vary by 2 to 3 orders of magnitude (Brantley and others, 2007). This variation in reaction rates will translate into the same order of uncertainty in the modeling of kinetically controlled geochemical processes. Especially in the area of geo-engineering and environmental protection these uncertainties can become inacceptable when stringent safety criteria or high costs apply. For example, prospective carbon capture and sequestration strategies rely on a fast ($<$10 y) conversion of CO_2 into carbonate minerals. These fast rates have to be confirmed and understood both at laboratory and field scales (McGrail and others, 2017). On the other hand, the programs for geological disposal of radioactive waste have to ensure protection of the environment from radiation on a time scale of 10^5 to 10^6 years.

Taking into account the system's complexity, we believe that a breakthrough in the quantitative description of the mineral reactivity in complex mineral systems can only be achieved with due account for the mechanistic understanding of the reaction-controlling processes and their couplings. The key factors controlling these processes are:

1. The atomistic mechanism of surface reactions and molecular mass transport
2. The chemical speciation on surface sites and in the near-surface fluid
3. The morphology and reactive site density of mineral surfaces
4. The pore-scale transport and the pore space evolution
5. The macroscopic mineral reactivity and rock textures

The main challenges for an integrated mechanistic description of precipitation/dissolution phenomena are the process couplings and the transfer of parameters controlling the system evolution between different scales. There are several examples of coupled reactive transport studies performed at various levels of details and scales, but none provides a satisfactory link between the reaction mechanism, the surface area evolution, and the macroscopic reactivity [for example, Steefel and others (2015b)]. A complete multiscale process coupling has not yet been obtained so far.

In the following sections we review the scale dependent phenomena related to the mineral fluid reactivity, and shortly discuss the strengths and challenges of the currently applied simulation methods. Where possible we discuss connections with

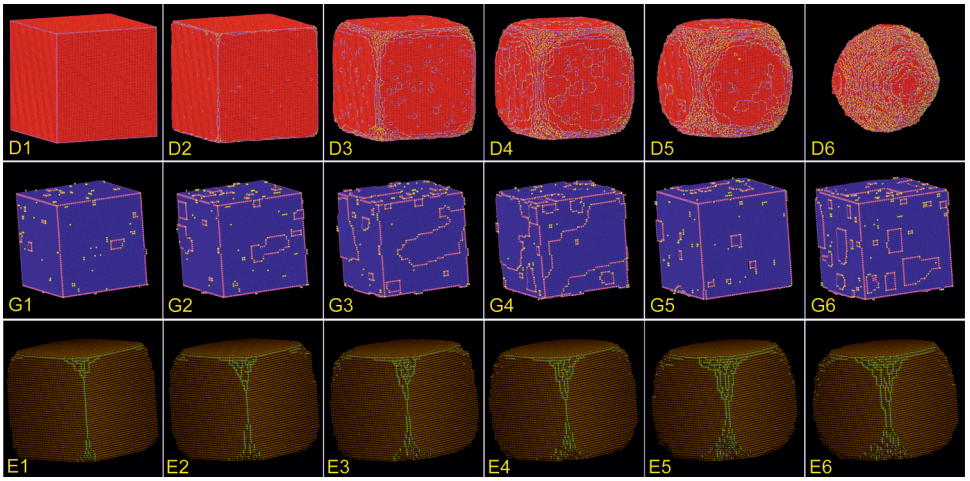

Fig. 1. Kinetic Monte-Carlo simulations of dissolution (red terrace sites), growth (blue terrace sites), and steady state dissolution/growth (brown terrace sites) for a dislocation-free Kossel crystal. Simple cubic lattice with nearest neighbor interaction is considered. The energy per bond is set to $4kT$ units, where k is the Boltzmann constant and T is temperature. All simulations start from the ideal cubic crystal shape. Pink and green/yellow colors mark step and kink/ad-atoms sites, respectively. At highly under-saturated conditions, the dissolution of the perfect crystal starts with a spontaneous etch pitting of the cubic {100}, dodecahedral {110} and octahedral {111} faces. Soon after, the dissolution at {110} and {111} takes over as a consequence of higher defect density, leading to a round-shaped dissolving solid grain. In a steady state regime close to the equilibrium conditions, the etch pitting of {100} faces is suppressed by re-healing. A concurrent dissolution-precipitation dominates at {110} and {111} faces and results in a stabilization of cub-octahedral crystal habitus. The growth of a dislocation-free crystal is initiated by an attachment of ad-atoms to {100} faces, and proceeds by a stepwise filling of the {100} monolayers. The crystal maintains the cubic habitus.

phenomena at neighboring scales and bring examples from our work and from literature. Thereafter, we critically discuss current status of process couplings, and describe further requirements for an upscaling and downscaling of the reactive transport relevant phenomena.

ATOMIC SCALE PROCESSES

Most of the sparingly soluble minerals grow and dissolve via the advancement of atomic steps on the reacting surface (Lasaga and Blum, 1986). The retreat or advancement rate of a single step depends on the activation energy for detachment and attachment of structure-forming ions from or to the surface, respectively. Figure 1 shows a limiting case of dissolution, growth and a steady state dissolution-precipitation of a Kossel crystal, obtained by kinetic Monte Carlo simulations, considering only the binding energy in the first coordination shell of the reactive sites. Even such a simple model shows principal differences in the evolution of crystal surface morphology during the dissolution, growth and steady-state dissolution-precipitation equilibrium dynamics.

From the energy point of view, the kink and the terrace sites are the most and the least favorable sites for the dissolution, respectively. The dissolution of defect-free {100} crystal faces, far from the edges and corners, is initiated by a “nucleation” of single-defect etch-pits. The overall material flux from the surface is, however, dominated by the dissolution from dodecahedral {110} and octahedral {111} faces. At the advanced stage of the dissolution, the crystal takes a spheroidal shape. The surface maintains extremely high kink site density. Detailed analysis of the net dissolution rate, performed in KMC simulations of different minerals, indicates large temporal fluctuations

in the material flux from the surface (Lüttge and others, 2013; Kurganskaya and Luttge, 2016). These rate variations are related to the changes in reactive site density caused by an interaction of dissolution stepwaves originating in different special crystal locations.

The growth of a dislocation-free crystal is controlled by the nucleation of ad-atoms on terrace faces. Newly-formed steps propagate until the end of the crystal face boundaries, and the cycle repeats. {100} faces dominate the crystal habitus at any time. The principal difference between the patterns for dissolution and growth, dictated by the used model, is that in the former case, the edges and the corners of the crystal act as an auto-catalyzing source of highly reactive kinks, whereas no such auto-catalyzing process for the ad-atom generation is available on the dislocation-free crystal during the growth.

Because of high energy costs of formation of an ad-atom or a point defect, etch-pits are associated with large energy costs, and it is generally argued that the primary source of kink sites for the precipitation and growth are the screw dislocations (Lasaga and Blum, 1986). These have been observed *in situ* by AFM measurements (Teng and others, 1998; Teng and others, 2000; Putnis and Ruiz-Agudo, 2013). On the basis of dissolution energy, (Lasaga and Lüttge, 2001; Lasaga and Lüttge, 2003) have formulated a so-called step wave model that explains the formation of macrosteps, hillocks and larger pits, resulting in a complex and variable surface topography of mineral dissolution patterns. Therefore, the information on the kinetics of these processes and on the evolution of the surface topography is essential for the macroscopic description of the reaction rates (Lasaga and Lüttge, 2004).

The majority of KMC simulations, focused on dissolution of minerals at far-from-equilibrium conditions, approximated the activation energies for the reaction event by the strengths of chemical bonds (Kurganskaya and Luttge, 2013a; Kurganskaya and Luttge, 2013b; Kurganskaya and Luttge, 2016). Thus, the reaction probabilities were considered to be a function of the bond-breaking energy and not of the activation barrier. This is a legitimate approach, as long as only one process (for example, dissolution) is considered. In this case, relative probabilities of the reactive events depend on the sum of the activation and formation free energies for each event. In complex systems and in presence of concurrent dissolution/precipitation processes, surface reactions may proceed via several mechanisms, each described by different activation energies for the breaking and the neo-formation of interatomic bonds. The net reaction progress depends on the number of reactive sites with a different speciation, which is determined by the surface morphology and the thermodynamic conditions. The surface morphology, in turn, is influenced by the reaction history and is itself a result of competitive interactions between different reactive events. These phenomena and the speciation of the fluid at the interface have to be taken into account.

Free Energy of a Reaction Mechanism from Molecular Simulations

Atomistic modeling can be used to directly probe the mechanism and the free energy of surface reaction pathway (Churakov and others, 2004; Liu and others, 2012; Stack and Kent, 2015; Zhang and others, 2017). *Ab initio* molecular dynamics simulations of important geochemical reactions, such as de-hydration, carbonation or even sorption complexation, demonstrate that attachment and detachment of ions to the mineral surface is a complex multi-barrier event. One and the same ion can form distinct complexes with different denticity, sorption energies, and the corresponding activation barrier for the adsorption reaction (Churakov and Daehn, 2012; Kremleva and others, 2012; Liu and others, 2012; Zhang and others, 2018). Recent studies of calcite-water interface, for example, clearly demonstrate differences in the interaction of Ca^{2+} and CO_3^{2-} with terrace-, step-, and basal surface of the calcite. The simulations

suggest that direct adsorption of Ca^{2+} in the kink position is highly unfavorable. The adsorption probability for Ca^{2+} increases significantly when co-adsorption is followed by the primary uptake of CO_3^{2-} group (De La Pierre and others, 2016; De La Pierre and others, 2017).

Thermodynamic View on the Surface Speciation

The chemical speciation on the surface is one of the key parameters controlling the reactivity of mineral surface. The proton activity has been recognized as the most important factor governing the reactivity of rock forming minerals such as silicates and carbonates (Blum and Lasaga, 1988; Morse and others, 2007). The pH-dependent protonation/de-protonation reactions on oxygen surface sites influence the bond strength and the activation barrier of the surface reactions (Lasaga and Gibbs, 1990; Xiao and Lasaga, 1996). Macroscopically, the surface speciation is computed using thermodynamic surface complexation models (SCM) (Lyklema, 1995). In such models, the surface of the mineral is represented by a planar or at best a spherical interface. The surface reactive sites, typically oxygen atoms with uncompensated bond charge balance, are the source of the surface charge due to the protonation/de-protonation and ion adsorption reactions (Hiemstra and Riemsduk, 1996; Sahai and Sverjensky, 1997b; Pokrovsky and others, 2005; Wolthers and others, 2008; Pokrovsky and others, 2009; Oelkers and others, 2009; Wolthers and others, 2012). Depending on the SCM approach used, the ions at contact with the surface are considered either as the part of the diffuse double layer or as a part of the surface (see fig. 2). Several extensive reviews of the SCMs and their historical development exist in the literature (Lutzenkirchen, 2002; Kulik, 2009). The effect of the ion-ion interaction on the surface complexation reactions and protolysis is typically considered in a mean-field approximation (for example, as an average relative electrostatic potential resulting from the superposition of all single ion potentials).

In the MGC model (fig. 2), the amphoteric surface sites participate in protonation/de-protonation reaction, and the mobile ions are distributed in the diffuse layer according to the Poisson-Boltzmann equation. The surface potential is assumed to be equal to the contact potential in electrolyte at the interface. The standard state of the surface reaction is defined for the neutral surface and the intrinsic acidity of the surface sites. The effective surface complexation constant depends on the mean electrostatic potential due to the surface charge. The finite size of the surface sites and ions does not enter into model parameters explicitly, but, in principle, can be accounted for via the activity coefficient.

The TL model assumes that the (de-)protonated surface sites, inner-sphere complexes, outer-sphere complexes are located within a set of individual planes at increasing distance to the surface (fig. 2). The distribution of ions between the sorption sites is obtained by the speciation calculations. In currently most widely accepted TL model CD-MUSIC (Hiemstra and Riemsduk, 1996) the formula charge on each surface complex is distributed between 0, β and d planes according to the mineral specific constants. These charged planes form a series of parallel capacitors. The electrostatic potential in each plane contribute to the activity coefficients. Free model parameters are the surface complexation constants. Due to potentially strong correlation with the surface complexation constants the capacitance of two layers are not fitted but fixed constant at some physically meaningful value. The capacitance can be further broken down into the dielectric permittivity of the media and the distance between charged planes. It is, however, difficult to obtain an unambiguous estimation of all model parameters (Sverjensky, 2001; Sverjensky, 2005). Neither capacitance density nor the dielectric permittivity of the interfacial region can be directly measured (Cheng and Sprik, 2014). The model has been applied with success to a large number of systems (Sahai and Sverjensky, 1997a; Sverjensky, 2006). The thickness of the

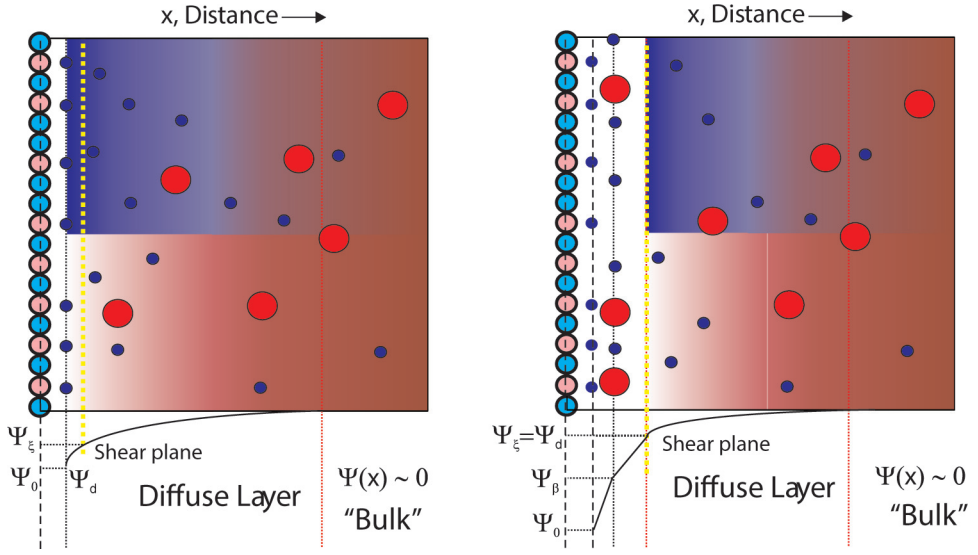

Fig. 2. Schematic representation of the modified Gouy–Chapman (MGC) model (left) and the triple layer (TL) model (right) (Lyklema, 1995). Surface sites are shown by pink [negatively charged,(−)] and light blue (zero charged) spheres surrounded by black circles. The net negative surface charge emerges due to deprotonation of surface sites, controlled by the pH in solution. The distribution of ions charge in the diffuse layer is described by Poisson-Boltzmann equation for external electrostatic potential $\psi(x)$. In the MGC model, the surface potential is equal to the contact potential of the diffuse double layer $\psi_0 \equiv \psi_a$. The TL model assigns the location of surface sites and inner-sphere complexes, the outer-sphere complexes and the contact of diffuse layer to three distinct surface plains with corresponding net charge densities (σ_0, σ_β, σ_d). Inner-sphere complexes are located in 0-plane. The σ_0 charge density is the sum of the charges contributed by surface sites and the inner-sphere complexes. The β-plane indicates the location of outer-sphere surface complexes, whereas the d-plane marks the beginning of diffuse layer. These charged planes form two sequential capacitors with the capacitance C_1 and C_2, respectively. The potentials at each plane are thus linearly related: $\psi_0 - \sigma_0/C_1 = \psi_\beta = \psi_d - \sigma_d/C_2$. The MGC model can be formally deduced from TL model setting the capacitance to infinity. The shear plane indicates a virtual boundary between "immobile" ions bound to the surface and "mobile" ones in the aqueous solution. The choice of the shear plane position is not constrained by SCM parameters and has to be tuned to independent data on ions mobility. In TL models the shear plane is often assumed to co-inside with d-plane.

sorption layers can, in principle, be estimated based on various spectroscopic methods (Hofmann and others, 2016). The distribution of ions between inner- and outer-sphere complexes may depend on the nature of the surface and on the electrostatic properties of bulk mineral, for example magnitude and the structural position of surface charge. The location of ions in the inner and outer-sphere complexes is a complex result of a balance between the surface-ion and ion solvent interaction.

Atomistic View on the Fluid Solid Interface

Molecular simulations provide insights into the nature of mineral-aqueous interface and allow discriminating the effect of mean-field electrostatic interaction of ions with the surface, dynamic ion-ion correlation phenomena, and the short-range steric effects at the interface. Figure 3 demonstrates the density distribution of water and ions in 1 M NaCl solution confined in a 2 nm wide slit pore between montmorillonite, pyrophyllite and kaolinite basal planes. Both montmorillonite and pyrophyllite have nearly identical arrangement of the surface sites. Pyrophyllite particles are charge-neutral, whereas montmorillonite particles carry a permanent negative structural charge due to the isomorphous substitution of Mg(II) for Al(III) in the octahedral layer. The negative structural charge in montmorillonite is balanced by excess sodium

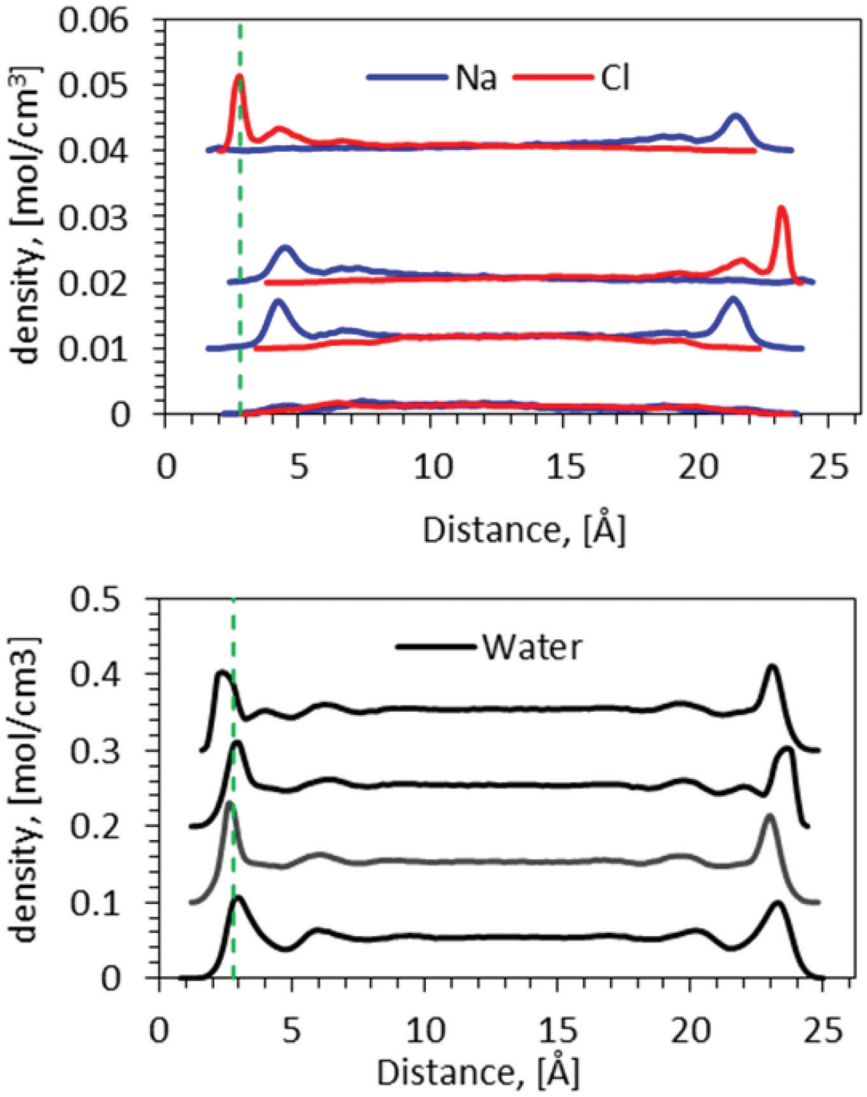

Fig. 3. Effect of surface charge and surface speciation on the structure of mineral-water interface and ion adsorption. Lines from bottom to the top: Pyrophyllite, Montmorillonite, Kaolinite (OH-surface to the right), Kaolinite (OH-surface to the left). Montmorillonite and pyrophyllite have similar structural arrangement of surface sites, but different surface charge. Whereas pyrophyllite particles are neutral, montmorillonite particles carry a permanent surface charge. Kaolinite, an uncharged clay mineral, has two non-equivalent surfaces: one is structurally similar to the surface of pyrophyllite and montmorillonite; another is composed of OH groups similar to $Al(OH)_3$ (gibbsite). The origin of x-scale corresponds to the position of the outermost oxygen atoms on the surface of each mineral. The green dashed line indicates the location of first water layer in montmorillonite water interface. The simulation details are given in Appendix 1.

ions present in addition to those in the background electrolyte. Irrespective of the surface charge, the water density profiles at the surface of two minerals demonstrate a clear similarity. At least two highly structured layers of water molecules can be distinguished at both interfaces. The position and amplitude of the maxima and minima of the density profiles are strikingly close. However, the ion density profiles are

entirely different. The concentration of outer-sphere surface complexes at the montmorillonite surface is by factor 3 higher compared to the background electrolyte concentration. In contrast, both Na^+ and Cl^- are depleted at the pyrophyllite water interface. The pyrophyllite water interface is essentially hydrophobic (Teppen and others, 1997; Tesson and others, 2016). Depletion of ions in the surface layer allows to optimize the structure of hydrogen bonds at the interface and to minimize the surface energy of the fluid. Based on the large similarity of water density profiles and, at the same time, substantial differences in cation distributions, one can conclude that the primary origin of the solvent structuring at the interface is the hydrogen bonding interaction between water molecules and the mineral surface, and the steric effects due to the alignment of water at the interface.

Kaolinite is an uncharged clay mineral with two distinct basal plane types. One basal plane is terminated by oxygen sites similar to the surface of pyrophyllite, whereas the second surface is covered by >OH groups similar to the aluminum hydrophyte gibbsite. One could intuitively expect similar sorption behavior for the oxygen-terminated basal plane of kaolinite and pyrophyllite. The simulations results contradict this analogy (fig. 3). The most prominent feature of the kaolinite-water interface is the adsorption of Cl^- anions as inner-sphere complexes on gibbsite-like surface. A closer examination of the ion density profile also reveals a minor fraction of co-adsorbed inner sphere Na^+ complexes and a large fraction of Na^+ outer-sphere complexes. Similar behavior of kaolinite-water interface has been observed in different electrolyte solutions (Vasconcelos and others, 2007). The kaolinite-water interface at oxygen-terminated surface is enriched with outer sphere complexes of Na and depleted in Cl^- similar to the montmorillonite-water surface.

Preferential adsorption of Cl^- ion on the hydroxylated surface of kaolinite can be explained by a cooperative motion of >OH groups at the surface and by electrostatic correlation effects. >OH groups have large orientation freedom and allow formation of strong tri-dentate complexes with Cl^- anion. Enrichment of negatively charged Cl^- ion at the same time promotes co-adsorption of inner-sphere Na^+ complexes. Accumulation of anions at the gibbsite interface breaks the charge neutrality in the slit pore and exerts a negative surface charge to the opposite basal plane of kaolinite particles. This surface potential, in turn, triggers an enrichment of the outer-sphere sodium complexes at the oxygen-terminated basal plane of kaolinite, similar to that observed on the basal plane of montmorillonite. This somewhat surprising charge separation within the slit pore solution is possible due to a much larger dielectric constant of water compared to the one of the solid.

The structure of kaolinite-electrolyte interface thus demonstrates that the site-specific ion surface interaction can lead to the accumulation of ionic charge even at the overall neutral mineral surface, and result in complex correlation between anionic and cationic densities next to the interface.

Another important aspect, often neglected in the studies of the interfacial phenomena in porous media, is the saturation. Especially during the weathering process, mineral fluid interfaces may undergo several de-/re-saturation cycles. Even at very low relative humidity, mineral surfaces remain covered with a thin water film, whose thickness controls the complexation of the counter ions on the surface. Figure 4 shows changes in the water density at the surface of clay mineral as a function of relative humidity. Highly-structured region of water is restricted to approximately 1 nm. Beyond this distance, the water density approaches the value characteristic to the bulk fluid. At partially saturated conditions, the surface is covered by a water film less than 1.0 to 1.5 nm thin. Remarkably, the water density in such a film is similar to the one observed at the saturated conditions. As water chemical potential decreases, the desaturation takes place in a stepwise manner, so that the water density profile near

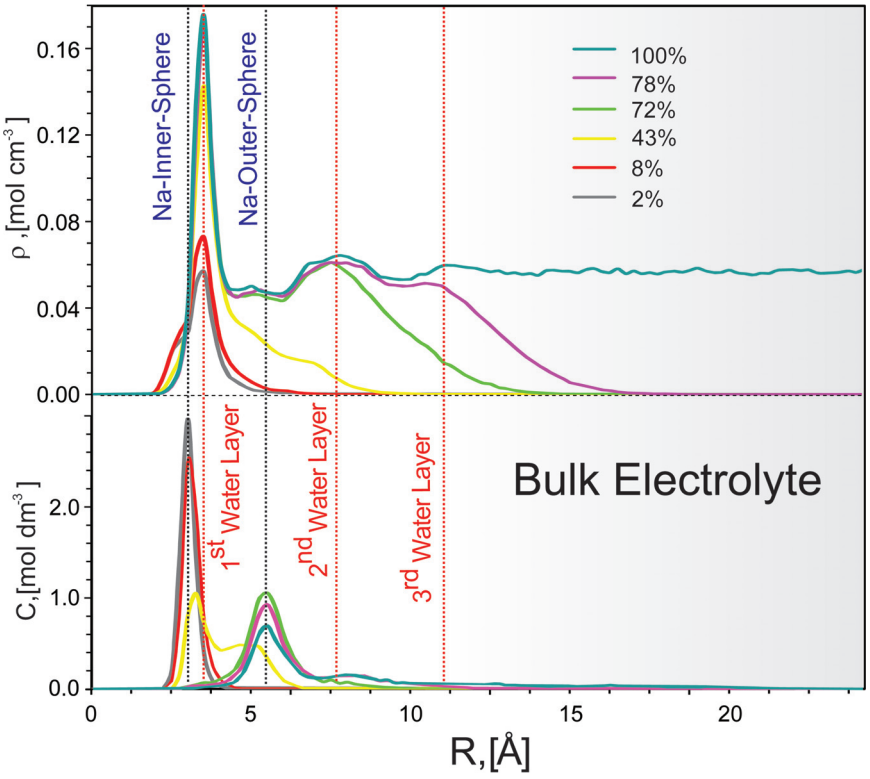

Fig. 4. Effect of water saturation on the ion-surface complexation mechanism of sodium ion on basal plane of montmorillonite, obtained with a combination of Monte-Carlo and Molecular dynamic simulation using the model of montmorillonite particle and SPC/E water model. See (Churakov, 2013) for the simulation details.

the surface follows the density observed in saturated conditions as far as possible. At fully saturated conditions, sodium ions prefer to maintain the water hydration shell and adsorb as outer sphere complexes that are predominant until the saturation drops to 50 percent relative humidity. At lower water potential, the surface complexation changes from outer to inner sphere complexes. This change is driven by the reduction of the water film thickness from 3 to 2 layers. By changing the complexation mechanism, Na is able to maintain six oxygen atoms in the first coordination shell down to extremely low saturation conditions. The change in the surface complexation mechanism has several consequences for the reactivity of the interface and the speciation. Firstly, the ion concentration in the immediate vicinity of the surface is increasing. The ions present at the surface are likely to promote bond polarization of the surface sites and to lower the activation barriers for the dissolution process. Secondly, the relative fraction of water molecules bound to the cation is significantly increased compared to the condition in a bulk fluid. The water – ion interaction is known to reduce the effective pK_w value for water molecules bounded to cations. The confined water has been shown to be more acidic compared to the bulk (Liu and others, 2011). The effect is further amplified with an increasing cation charge. Therefore, the thin water film on mineral surface will more readily deliver protons necessary for the bond hydrolysis.

Transport in the Near Surface Layer

The progress of surface reactions strongly depends on the availability of reactants that have to be supplied or removed from the fluid-mineral interface by advective or diffusive transport. On the larger scale, the fluid transport will be mainly determined by the texture of the rock and connectivity of the pore space. The description of chemical transport near the mineral surfaces is nontrivial. Even within the macroscopic advective regime, the transport near the surface can be diffusion controlled due to the formation of a diffusive double layer (DDL) at the charged mineral surfaces. The local mobility of ions close to mineral surfaces has been extensively characterized by molecular simulations. In general, an order of magnitude decrease in the mobility of adsorbed ions is observed compared to the diffusivity in the bulk (Kalinichev and Kirkpatrick, 2002; Wang and others, 2004; Wang and others, 2006; Marry and others, 2008; Botan and others, 2011; Churakov, 2013). The spatial extent of the DDL depends on the surface charge density and the solution composition. The interfacial fluid is enriched in cations and depleted in anions or vice versa depending on the sign of the surface charge density. This enrichment has consequences for reaction kinetics. Whereas the chemical potential (or activity) of the species in the DDL is constant and equal to that in the bulk (assuming of chemical equilibrium), the concentration is not the same. However, concentration rather than activity is the phase parameter in the kinetic equations. Considering the system complexity and the strong coupling between different processes, it is not surprising that the parameters in equations 1 to 3 are normally considered as simple fitting quantities. Equations 1 to 3 are very useful for interpolating experimental data but are obviously too simplistic to provide an insight into reaction mechanisms or used for extrapolation into a broad range of conditions beyond the experimentally available datasets.

Atomistic Description of Surface Speciation

The macroscopic SCM will not be able to incorporate all the aspects of the molecular scale interactions in satisfactory manner. Several attempts have been taken to challenge various SCM versus atomistic simulations and experimental data (Tournassat and others, 2009; Tournassat and others, 2013). The simulations show that the distribution of ions between inner and outer-sphere coordination is controlled by the relative strength of the ion-solvent and ion-surface interaction (Sverjensky, 2005). Thus, among the ions of equal ionic charge, the larger ions tend to loose solvent more easily and to form inner-sphere complexes. In the absence of specific, preferentially covalent ion surface interaction, divalent and trivalent ions tend to maintain their hydration shell and adsorb as the solvent-separated outer-sphere complexes.

The atomistic simulations with an explicit solvent provide most detailed information on the mechanism of ion - surface interaction at rather high computational costs. The typical size of the system includes $\sim 10^4$ to 10^5 atoms at best, and the time scale covered is restricted to a few nano seconds. The major flaw of the macroscopic SCM models, on the other hand, is their inability to give a proper account for the ion-ion correlations and the non-planar surface morphology. The ion-ion correlations become increasingly important for 1:1 electrolytes at higher, for example above 0.5 M concentrations, and become indispensable for 2:1 and 2:2 electrolyte (Valleau and Torrie, 1984). Several important effects related to the charge reversal of the ξ-potential can only be explained by the effect of ion-ion correlation. Coarse-grained simulations with an implicit solvent bridge the scale of fully atomic system description and macroscopic thermodynamic models (Labbez and Joensson, 2007; Labbez and others, 2011; Churakov and Labbez, 2017). Similar to the SCM model, the GCMC simulation considers the solvent as a dielectric continuum, but takes a full account for the finite ion size, the surface morphology, and ion-ion correlation effects in electrolytes. Figure 5 illustrates

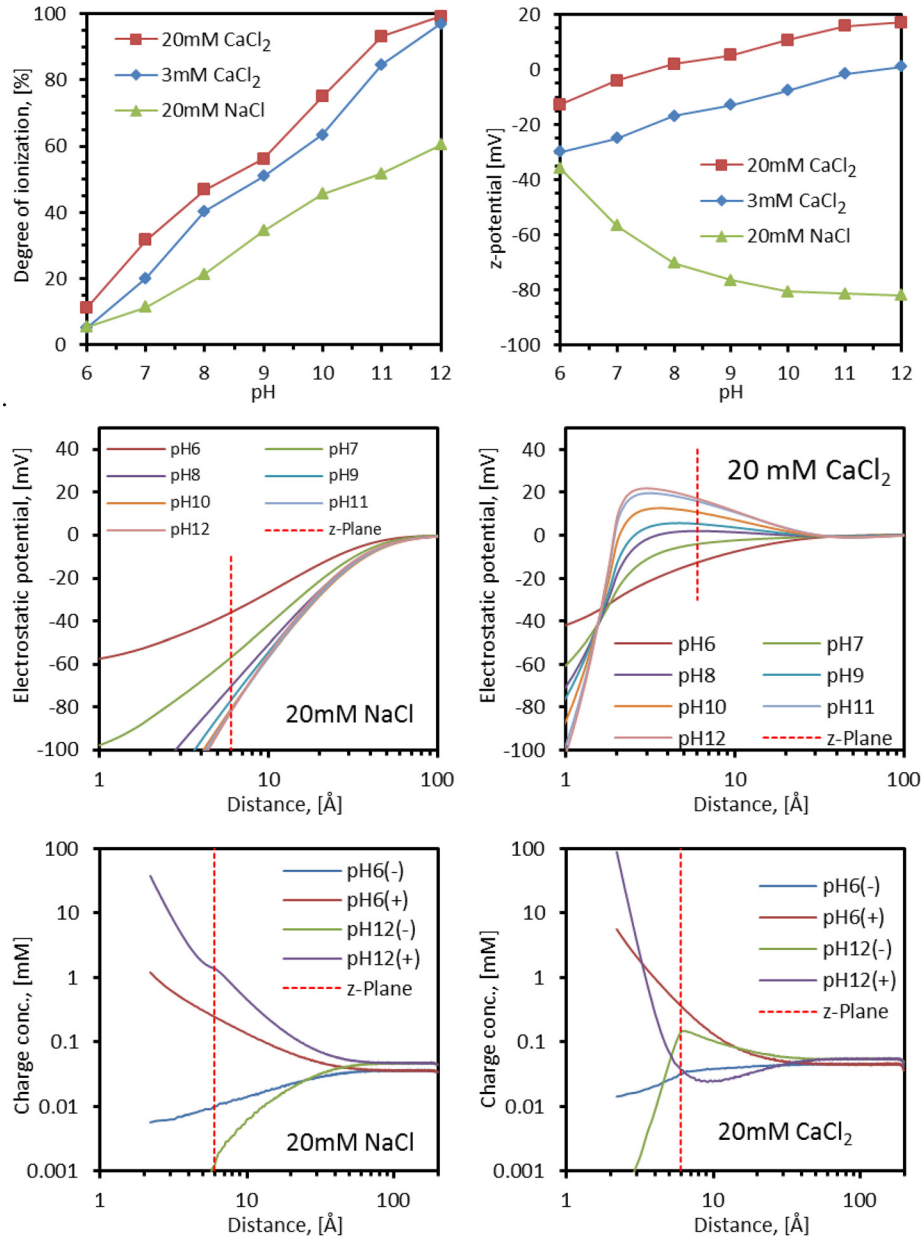

Fig. 5. ξ-potential, and surface charge at tobermorite surface in equilibrium with different electrolytes solutions obtained by GCMC simulations. Total charge density of positive (+) and negative (−) ions, and the concentration profiles of Ca, Na and Cl at the interface for Na and Ca dominated systems at 6 and 12 pH. The pH conditions are controlled by HCL/NaOH acid/base pair. Three systems are considered: 3 mM $CaCL_2$, 20 mM $CaCL_2$, mixture of 20 mM NaCl and <1 mM $CaCl_2$ (indicated as 20 mM NaCl) background electrolyte. Two lower charts show electrostatic potential for NaCl and $CaCl_2$ dominant system. The mineral surface is represented by >OH groups according to the mineral structure with intrinsic pKa constants 6.15 and 8.85 as obtained by *ab initio* molecular dynamics simulations (Churakov and others, 2014). The position of shear plane is shown by red dashed line.

the surface speciation, electrostatic potential and ion distribution on the surface of hydrous chain silicate mineral tobermorite ($Ca_4Si_6O_{15}(OH)_2$) in NaCl, $CaCl_2$ and in mixed NaCl/$CaCl_2$ rich fluid obtained by grand canonical Monte Carlo (GCMC) simulation (see Appendix 2 for technical details). Tobermorite is considered as a model for cement minerals, but can also be viewed as a prototype for other natural chain and group silicates. The model system is represented by >OH groups attached to Si-tetrahedra pairs. The acidity of the two >OH group types present at the surface (pK_a), was evaluated by *ab initio* molecular dynamics simulations as 6.15 and 8.85 (Churakov and others, 2014). With increasing pH, >OH groups at silanol sites deprotonate, and the surface becomes negatively charged. The deprotonation of >OH groups creates the surface charge, which stimulates cation adsorption. The surface potential and charge distribution is very different in NaCl and $CaCl_2$ solution. At a given value of pH, the surface ionization more readily occurs in the Ca rich solution and results in higher surface charge density compared to the NaCl system. In NaCl solution the electrostatic potential monotonically drops with increasing pH. The value of electrophoretic potential remains negative. In the Ca rich system, the value of electrostatic potential at a distance of few ionic radii to the surface (for example, at the location of shear plane) increases with increasing pH and eventually leads to the sign reversal of electrophoretic potential (ξ). This charge reversal is attributed to the adsorption of Ca ions at the interface which over-compensate the negative surface charge. The positive potential in turn promotes the co adsorption of anions at the interface. This effect is clearly seen on the charge density profile for $CaCl_2$ system at elevated pH. Contrary to intuitive expectation the negative charge concentration at the location of shear plane in larger than that of the positive charge. Comparison of the Ca and Na rich system shows that this phenomenon is specific to 2:1 electrolyte and does not occur in 1:1 system even at high electrolyte concentration. The observed charge reversal in diffuse double layers is exclusively related to dynamic ion-ion correlation and cannot be captured in a mean field approximation (Torrie and Valleau, 1982). It can be concluded in general that highly charged cations lead to stronger surface ionization for the same pH conditions. It is therefore to expect that the concentration of divalent cations must have significant effect on the hydrolysis of surface sites and thus on the dissolution kinetics.

PORE SCALE PROCESSES

A step higher in the hierarchy of the characteristic length scales, lies the pore scale. The main advantage of a multi-physics pore-level model, is the fundamental description of geochemical reactions in realistic structures subject to diffusive or advective mass transport. Compared to macroscopic methods, the direct access to primitive variables, such as the reactive surface area (it is known exactly) allows to describe accurately the pace of reactions (kinetics). Alterations of the pore-space and its connectivity, due to dissolution and precipitation, can be correlated with the change of transport properties. For example the formation of nanometer to micrometer-sized precipitate layers around preexisting mineral grains, dramatically reduces the permeability of the medium. This affects the macroscopic flow through it, although the total porosity does not change significantly. Flow alteration has in turn an effect on mineral precipitation-dissolution processes indicating a fully coupled hydro-geochemical reactive transport process. At this scale, the simulation of the diffusion and reaction processes at the pore-space, when surface charges play an important role, is also possible. Representative pore structures can be computer generated, or can be obtained via synchrotron based micro-tomography techniques. When combined with appropriate reaction and thermodynamic models, they can be used to support the interpretation of experiments and to fit transport parameters of interest. Moreover, the output of a pore-level simulation has the potential to be up-scaled and used

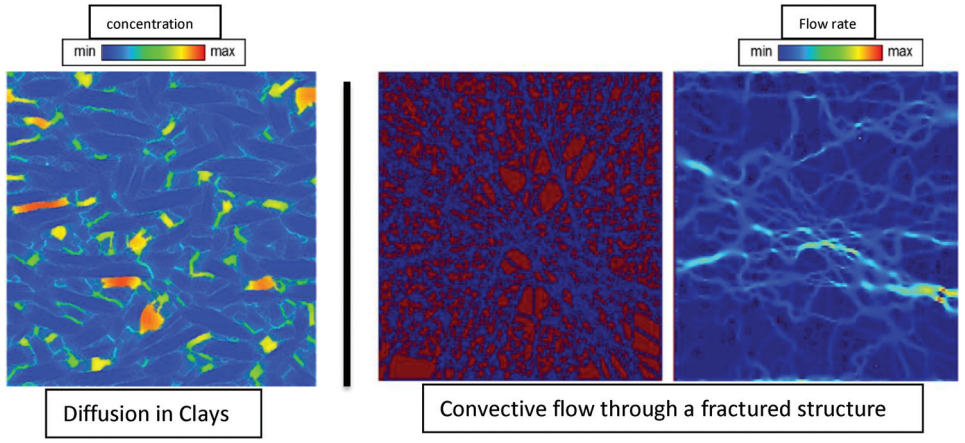

Fig. 6. (Left) Diffusion dominated transport in a clay structure; (right) convective flow through a random fractured structure where preferential flow paths indicate the locations of high mass transport.

together with the established macroscopic codes in order to improve their predictive capability.

Depending on the desired level of the physical and chemical description, several methodologies can be applied. Such an example, is the Pore-network models, which show advantages when large systems and relatively simple physics are considered. This is due to the inherent simplification of the pore geometry to equivalent pores and throats where physics are solved (Blunt, 2001; Hughes and Blunt, 2001; Raoof and Hassanizadeh, 2010). The more detailed pore-level methods solve the involved flow equations, or some approximation depending on the flow regime and the flow physics, in realistic geometries. These methods can include more complex structures, with complex interactions between species and phases, at the expense of computational cost when compared to pore-network models. Detailed pore-level models for geochemical reactions are based on the Lattice Boltzmann method (Kang and others, 2002; Parmigiani and others, 2011; Huber and others, 2014), on particle hydrodynamics (Tartakovsky and others, 2007; Chatelin and Poncet, 2013), as well as on the standard finite volume methods when applied in complex geometries (Molins and others, 2012; Trebotich and others, 2014; Soulaine and Tchelepi, 2016).

Among other parameters, the evolution of a porous geometry due to mineral reactions depends strongly on the mass transport flow regime. The quantification of these conditions is aided from dimensional analysis. The non-dimensional numbers that are used to characterize geochemical reactive flows, which are dominated by diffusion and advection, at the Darcy convective flow regime are the Peclet number: $Pe=UL/D_0$, and the Damköhler number: $Da=kL/D_0$, where D_0 is the mass diffusivity, k is the reaction constant, U is the convective flow velocity and L is the characteristic linear dimension of the system of interest. For faster flow rates the mass inertia effects start dominating the flow, and the Reynolds number ($Re>1$): $Re=UL/\nu$, where ν is the viscosity of the fluid, has to be considered as well.

In figure 6 two examples of mass transport regimes in different pore geometries, obtained by pore scale lattice Boltzmann simulations are shown. On the left, a snapshot of a generic diffusion dominated migration of ions from macro-pores into interlayer pores in clay minerals is shown. The clay structure is constructed according to the methodology of (Tyagi and others, 2013) which allows generating heterogeneous anisotropic structures, which are composed of different types of grains. Diffusion

proceeds along the large pores as well as along the interlayer-structure of the grains and the local concentrations are plotted. On the right, the advective flow field in a random generated fractured structure is shown. The flow is driven by the presence of a pressure gradient (direction from left to right). High flowrates signify the preferential flow paths, where most of the mass transport occurs. In a reacting environment, where fluid-solid interaction results in a change of the pore-space and its connectivity, the diffusion and advection paths will dynamically change.

Time dependent evolution of porosity and pore connectivity by dissolution (for example acid injection in calcite rock) can be categorized using the aforementioned non-dimensional numbers (Fredd and Fogler, 1998; Golfier and others, 2002; Szymczak and Ladd, 2009; Battiato and Tartakovsky, 2011; Kang and others, 2014). Numerical models can reproduce to a certain degree experimentally observed patterns as for example the formation of the so-called wormholes. The different evolution paths that a system can follow, for example during dissolution, indeed show that the transport properties of an evolving porous structure due to reactions are not solely functions of the porosity, the reactive surface area and the tortuosity. This implies that Kozeny-Carman relation, for permeability, and Archie's law, for effective diffusivity, are not accurate in the case of geochemical reactive transport especially under the presence of strong chemical gradients. For that reactive transport pore-level simulations with appropriate geometrical input (computer generated structures / tomograms) pave the way for extracting such correlations (Prasianakis and others, 2018).

Lattice Boltzmann Framework

The lattice Boltzmann method is a special discretization of the Boltzmann equation which originates from the gas kinetic theory (Frisch and others, 1986). The elementary variables are the so-called populations, which represent the probability of finding a particle with a given velocity and particular location in space. At every lattice point the distribution function is represented by a set of discrete velocity vectors (Succi and others, 1989; Qianand others, 1992; Succi, 2001). Such models are shown to recover the full Navier-Stokes equations. This essentially allows to use exactly the same model and algorithm both to Darcy flow regimes (Reynolds < 1), as well as to high Reynolds number flows, as for example the kind of flows expected within fractures. A remarkable advantage of the lattice Boltzmann methodology, is the minimum effort to discretize a realistic computational domain combined with the possibility to efficiently update the continuously evolving boundary of the solid structure, as for example in simultaneous dissolution and precipitation processes (Kang and others, 2006; Prasianakis and others, 2017). Given a specific structure the permeability and diffusivity can be measured exactly in a numerical way, with accuracy similar to the one of an experimental technique (Rosen and others, 2012). By construction, the lattice Boltzmann algorithm can be efficiently parallelized and used in high performance computing facilities (HPC). Moreover, the simplicity of the algorithm allows to exploit the computational resources based on general-purpose graphics processing units (GPGPU) (Safi and others, 2017a; Safi and others, 2017b).

The complexity in predicting the evolution of a system that undergoes simultaneous dissolution and precipitation reactions, were highlighted in the experiment and subsequent macroscopic modeling of the reactive flow experiment (Poonoosamy and others, 2015). In this experiment, a baryte-celestine system ($BaSO_4$-$SrSO_4$) was selected due to its relative simplicity and availability of thermodynamic data. A reactive zone was filled with celestine crystals with bimodal grain size distribution (<63 μm and > 200 μm) as modeled and shown in figure 7 (left). Under the presence of a $BaCl_2$ solution, the celestine crystals dissolve and baryte precipitates start to form. Baryte precipitation follows two distinct precipitation paths, depending on the saturation index (based on $BaSO_4$) of the solution and forms either nano-crystalline precipitates,

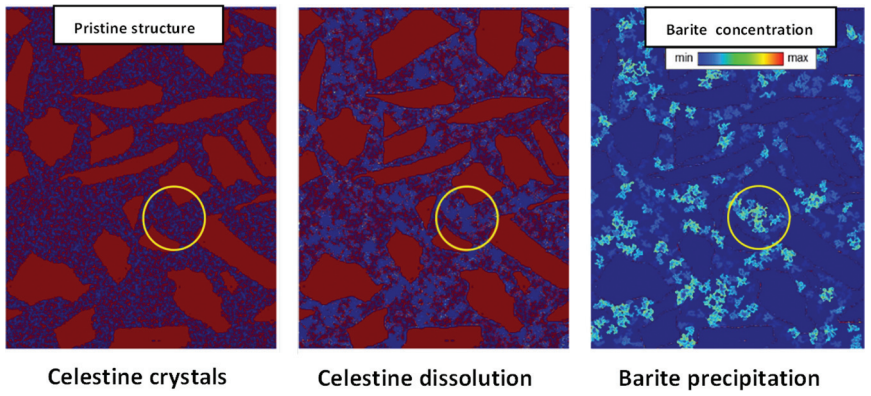

Fig. 7. Cross-scale simulations of concurrent dissolution and precipitation in a Baryte-Celestine system coupling classical nucleation theory and heterogeneous growth. Celestine crystals (red) dissolve (middle) and baryte precipitates fill the pores (right). Among other, pore size dependent kinetics of precipitation favors the onset of precipitation in larger pores (yellow circle).

or epitaxially grown precipitates (Poonoosamy and others, 2016), in a way that can be described by classical nucleation theory (Kashchiev and van Rosmalen, 2003; Prieto, 2014). The cross-scale modeling of (Prasianakis and others, 2017) combined the classical nucleation theory for precipitation with advanced lattice Boltzmann multicomponent reactive models (Prasianakis and others, 2009; Kang and others, 2014), and allowed to reproduce the major experimental observations. Among other, the model takes into account the higher probability of the nucleation in larger pores as illustrated by the simulations results at high saturation index in figure 7 (middle and right). Such effects, while they are important, due to their complexity are usually neglected in the geochemical reactive transport modeling. For these simulations, precipitation follows the classical nucleation theory and possible heterogeneities on the crystal surfaces are not considered. The growth of primitive nuclei in the bulk, as well as on the celestite surfaces is implemented via a lattice subgrid model. Parametrization of the nucleation model is based on independently conducted baryte precipitation experiments and are obtained from the literature or calculated analytically for the system under consideration. In more complex systems, where experiments are not available, and if the surface heterogeneity needs to be taken into account, the parametrization of the subgrid model can be based on atomistic and kMC simulations.

The effect of precipitation on the transport properties of a porous structure can be a strong non-linear process, especially under the presence of substantial concentration gradients. To highlight this phenomenon, we here use the model developed by (Prasianakis and others, 2017) with the same parametrization, to simulate baryte precipitation in a computer generated porous inert structure with initial porosity $\varepsilon=0.497$. The reactive transport setup, the boundary conditions and the baryte precipitation distribution are shown in figure 8. A $BaCl_2$ rich solution diffuses from the left boundary to the right boundary, while a $NaSO_4$ solution from the right boundary to the left. The considered domain is a 1 mm $\times$ 1 mm two-dimension pore structure. Two cases with slightly different initial concentration gradients are shown. The initial concentration for the two simulation cases was set to both left and right boundaries at 0.5 M in the first case, and 0.1 M in the second case, with zero concentrations inside the pore-structure domain. In such a setup, the mass transport is governed by diffusion. The diffusion fronts meet after some characteristic time, and precipitation starts as soon as the induction time has passed for the respective saturation index. Two

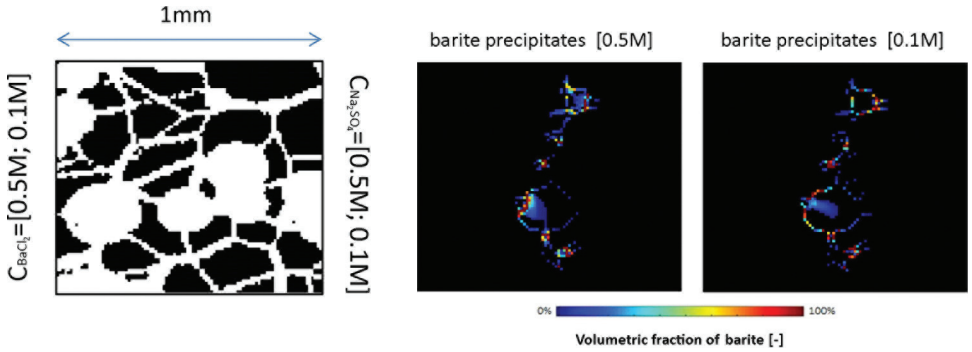

Fig. 8. Left: Initial pore structure and the boundary concentrations for the diffusion controlled simulations with 0.5 M and 0.1 M concentration of solutes on the boundaries; Middle: Volumetric distribution of baryte precipitates which results in clogging of the pore network obtained for the 0.5 M boundary condition. Right: A snapshot representing the same amount of precipitate (as the middle 0.5 M picture) obtained in the simulations with 0.1 M boundary conditions. A longer reaction time is needed to obtain the same amount of precipitate. At this time, the 0.1 M case porosity remains still interconnected.

different baryte solid phases are formed approximately in the mid-plane of the domain, something that is also observed in such experiments. Evolution of the system for the two cases is morphologically different, and depends on the relative rate of homogeneous versus heterogeneous nucleation, which produce nanocrystalline-baryte and expitaxially-grown-baryte respectively.

The interplay of homogeneous and heterogeneous nucleation mechanisms which result in the precipitate formation is plotted in figure 9 as function of time, for two different boundary conditions. The horizontal axis represents the reaction time normalized to the time needed until the 0.5 M case clogs (approximately 30 h). The 0.1 M case clogs after a five times longer period due to the weaker concentration gradients. The vertical axis represents the amount of baryte precipitates and is normalized to the final amount of precipitates that result in the clogging of 0.5 M-case. For the 0.1 M case, a slightly larger amount of precipitates is forming until it also clogs. Nanocrystalline formation is favored at higher saturation index and both homogeneous and heterogeneous nucleation mechanisms produce baryte precipitates. The contribution of each mechanism is also plotted in figure 9. This highlights that both mechanisms are significant for the 0.5 M case, while for lower concentrations (0.1 M) the heterogeneous nucleation mechanism that produces epitaxially grown baryte prevails, as expected for a lower saturation index.

The transport properties of the evolved porous structure can be measured numerically since the exact evolved geometry is known at all times. We here measure the permeability similar to (Prasianakis and others, 2013). The evolution of permeability with respect to the changing porosity due to precipitation is plotted for both cases in figure 10. In both cases the porosity is clogged by a thin zone of baryte precipitates. A small amount of precipitates is able to disconnect the domain into two chambers, separated by an impermeable precipitate layer after a short reaction time. This zone is slightly more spread in the 0.1 M case. The total change in the porosity of the entire domain is less than two percent. However, this extremely small amount of precipitate is sufficient to drop the values of permeability and diffusivity to zero. This abrupt drop of the value of permeability cannot be fitted by a Kozeny-Carman type of correlation nor can be predicted *a priori* without running the actual simulation. The same holds for effective diffusivity, tortuosity and Archie's law.

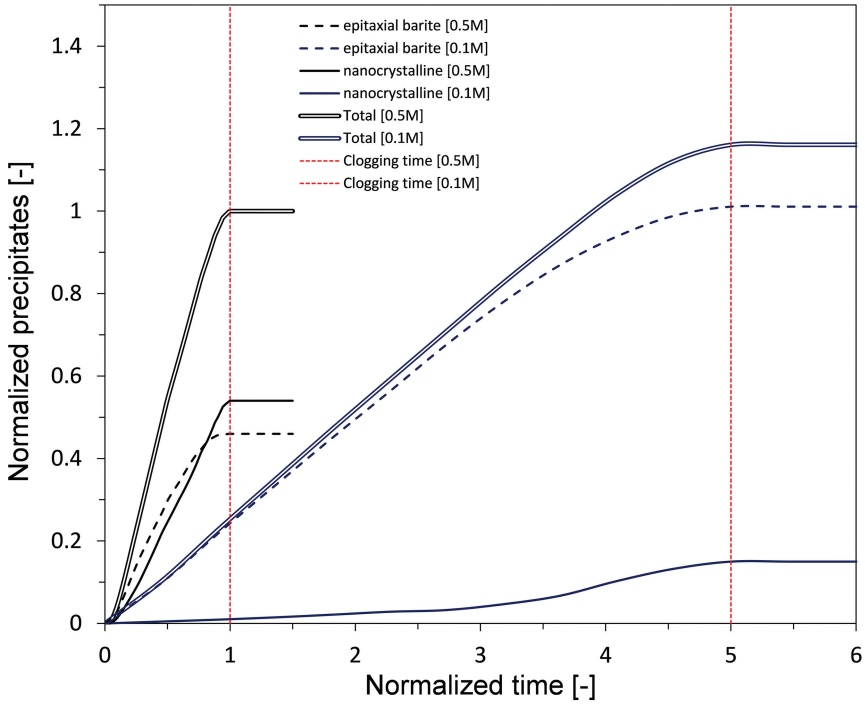

Fig. 9. Time dependent contribution of homogeneous and heterogeneous nucleation mechanisms resulting in formation of nanocrystalline and epitaxilly grown baryte for two different boundary conditions (see text for details). Crossover of the dominant mechanisms is observed for the case of 0.5 M. Both conditions result in disconnected porosity and halt of the reactions. Clogging time is highlighted with vertical dashed red lines for each case.

CHALLENGES FOR PROCESS AND SCALE COUPLING

A review of the major transport relevant processes was given in the previous sections, and demonstrates the significant progress that has been made over the last years in the detailed description of mineral reactivity and mass transport in natural systems. Various modeling tools are available, which can describe scale specific aspects of the mineral fluid reactivity even at the atomic scale in full detail. Many of these advances have become possible due to the steady increase of computing performance, which typically double each year as predicted by Moor's law (Moore, 1998), as well as due to the improvement and development of numerical methods and algorithms. Currently, the available computer resources allow testing the convergence of available simulation methods with respect to the system size, and to perform full 3D simulations of realistic domains in the case of transport simulations.

However, the coupling between modeling techniques addressing different length and timescales remains very challenging. The most attractive approach, but practically not feasible, would be a direct on-the-fly coupling between molecular and pore scale description of reactive systems, or between the pore-scale and continuum scale simulations. The efficient implementation of such a direct coupling for a realistic 3D system will not be feasible with current and near future computing technologies. The main obstacles are not only related to computational performance but also big data volumes that are needed for the detailed system description and analysis.

A pragmatic and efficient solution to the upscaling and downscaling problem must rely on scale specific parametrization of effective parameters (for example eqs.

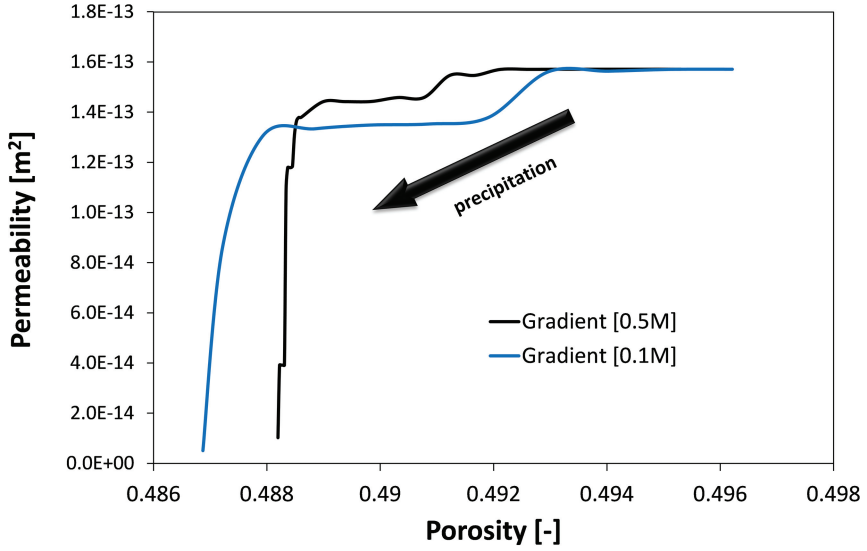

Fig. 10. Evolution of permeability with respect to the porosity changes as a result of precipitation for the cases of high (0.5 M) and low (0.1 M) concentration boundary conditions. Small changes in total porosity can result in dramatic decrease of permeability depending on the location of precipitates. For the same pore structure the evolution of the system depends on the chemical gradients.

1–4) based on sophisticated atomistic or pore scale simulations. Figure 11, illustrates the relationships between scales and scale dependent parameters. These parameters can be passed to the next coarser scale in form of a parametrized equation or using appropriate interpolation schema. In the following section we discuss the most important process couplings which could dramatically improve the description of reactive transport processes in the coming decade.

Atomic Scale Description of Complex Chemical System: Coarse-Grained Modeling Approach

Atomistic simulations provide most detailed description of the chemical system. In the same time the high level of detail becomes a drawback when complex systems are considered. In fact specific atomic scale processes have distinct characteristic time scale and can be efficiently decoupled using appropriate coarse-grained description of the system. Using the thermodynamic formalism of reference state the dependence on the concentration can be further obtained.

Quantum mechanical simulations are indispensable for the elucidation of reaction mechanism and for evaluating the activation energies of mineral reactions. The system size which could be practically treatable in such simulations is limited to few hundred atoms. This is however sufficient to set up a system with 1 M electrolyte solution, or a corresponding mineral fluid interface. Such a concentration scale is also a convenient reference state for thermodynamic calculations.

Chemical reaction relevant to the dissolution precipitation (for example, bond breaking-bond formation) can involve several solvent molecules from the first solvation shell of the reacting surface site and one or two solute species. The reaction itself is strongly localized in space. Only the species in the immediate vicinity of reactive site (for example, the first coordination shell) are directly involved in the reaction. Thus the intrinsic (defined for a reference concentration) reaction mechanism and thermodynamics properties of reaction can well be modeled in setup with just a few hundred atoms.

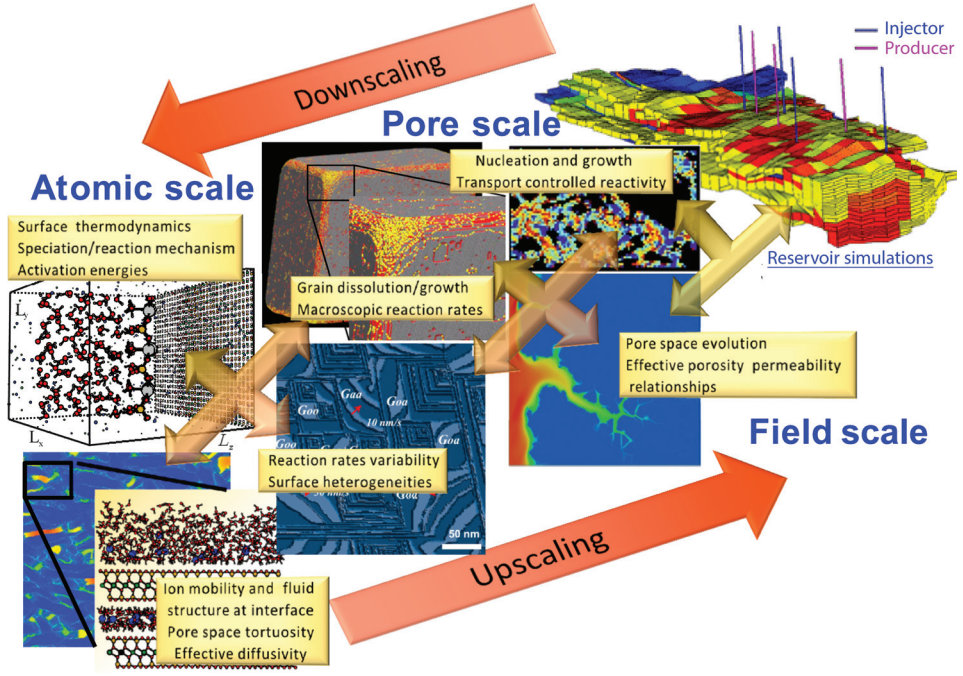

Fig. 11. Hierarchical coupling of processes and scales. Atomic scale modeling provide effective parameters for pore scale simulations such as activation barriers for surface reaction and the reaction mechanism (Churakov and others, 2004), thermodynamic properties of individual surface sites (Churakov and others, 2014), mobility of solvents and solutes at the mineral fluid interface (Churakov, 2013). This information is used by pore scale methods to simulate reactivity of individual mineral grain taking into account the heterogeneities of the mineral surface and variability of individual reaction rates (Kurganskaya and Luttge, 2016) and transport of fluid in the pore space (Tyagi and others, 2013). The evolution of pore space is predicted (Prasianakis and others, 2017) and the effective permeability and diffusivity of the porous media is evaluated (Prasianakis and others, 2018). These effective transport parameters are the input for the continuum scales simulation which can be applied for a broad range of applications from geothermal system modeling to large scale reservoir simulations (www.cpge.utexas.edu/?q=rp_ressim). The figures are adopted with permission from Journal of Physical Chemistry (2014), (2016), Scientific reports (2017), Geofluids (2018).

The concentration dependence of thermodynamic properties is related to the probability of reactants to meet in a close proximity so that the species can participate in a chemical transformation. These "collision probabilities" are controlled by long range coulombic interactions (ion-ion correlations) and steric effects such as surface topology. Therefore concentration dependent probability distribution function defining the likelihood for reaction to occur, can be evaluated based on a simplified model considering atom or molecules as charged particles interaction with long range coulombic potential and short range repulsion. These probability distributions are obtained by classical molecular dynamics and Monte Carlo simulations, and offer a way for obtaining pore scale transport parameters of solvent and solute molecules needed in pore scale simulations.

Surface and Fluid Speciation at the Interface vs. Surface Reactivity

Coarse grain simulation of surface reactivity such as kinetic Monte Carlo approach has been very successful in simulating changes in minerals surface morphology and evaluating material fluxes due to the dissolution and precipitation. Currently, the most advanced mechanistic models assume that the reaction mechanism is controlled by the

local coordination environment of the surface reacting species as defined by the crystallography of the bulk solid phase (Zhang and Luttge, 2007; Kurganskaya and Luttge, 2013a; Luttge and others, 2013; Kurganskaya and Luttge, 2016).

A necessary, improvement of the existing models would require an explicit consideration of the changes in the surface speciation, depending on the chemical condition and the fluid composition at the interface (fig. 7A). In a first step, the surface speciation can be taken into account based on the macroscopic surface complexation models (Pokrovsky and others, 2005; Pokrovsky and others, 2009). For many natural minerals and silicates in particular, the dissolution kinetics is controlled by protonation/deprotonation of anionic sites. Explicit consideration of the surface speciation as function of chemical conditions will allow accounting for the changes in the reaction mechanism depending on the fluid composition. The models based on the macroscopic surface speciation do not provide explicit molecular scale of the surface but only an average number of sites with the different speciation. These models will have a limited predictive power but can be very successful in interpolating the experimental data.

Explicit consideration of surface speciation can be done combining Grand canonical simulation of surface speciation with Kinetic Monte Carlo modeling of surface topography. With this approach the speciation of the surface sites can be obtained for an arbitrary surface topology. Moreover, the molecular simulations provide information about the coordination of the surface sites by fluid species. These data can be included into parametrization KMC model parameters.

The composition and intrinsic mobility of solvent and solute at the interface is not the same as in the bulk. Molecular simulations allow evaluating the specific mobility and ions at the interface. These data are used in the pore scale simulations to evaluate the integral effect of the near surface mobility and complex tortuosity of pore space (Rotenberg and others, 2007a; Rotenberg and others, 2007b; Rotenberg and others, 2010; Botan and others, 2011; Churakov and Gimmi, 2011; Tyagi and others, 2013).

Intrinsic Variability of Surface Reactivity

Analysis of data for mineral dissolution/precipitation reactions obtained with different techniques, which are based on distinct sample preparation approaches, reveals large quantitative discrepancies in the experimental results. These differences are likely to reflect the space-dependent variations of reaction mechanisms and the corresponding reaction rates. At different stages of fluid rock interaction, different mechanisms can dominate the reaction pathway. At the geological timescale or in the macroscopic experiments an average reaction rate is recorded as superimposed contributions of different reaction mechanisms. Analysis to time dependent material fluxes from mineral surfaces enables to reveal the contribution of individual reaction mechanism and their kinetic rates. Such analysis has been recently performed for different systems and has been manifested as the so-called rate spectra concept (Fischer and others, 2014; Fischer and others, 2015; Fischer and Luttge, 2017). To account for spatial and temporal coupling of reaction heterogeneities, "rate spectra" can be directly implemented into pore scale description of mineral reactivity. Coupled together with the pore scale fluid transport, the macroscopic composition dependent reaction rates for the continuum scale simulation can be derived.

Reaction Rates, Structural Heterogeneities and Reactive Transport Pathway

Scoping calculations for different types of porous media demonstrate that the propagation of reactive fronts depends on heterogeneities and reaction rates in a strongly non-linear way. Especially in the regime of high Pe and Da numbers the reactive fronts follow preferential transport pathways (Fredd and Fogler, 1998; Golfier and others, 2002; Szymczak and Ladd, 2009; Battiato and Tartakovsky, 2011). Injection

of undersaturated fluid in porous media in high Pe-high Da regime can result in formation of wormhole pattern (Prasianakis and others, 2018), while an oversaturated fluid favors the formation of dendrite like precipitates (Tartakovsky and others, 2007). Despite the strong non-linear relation between the transport and reactivity, a system study can be based on numerous statistical realizations of porous media, with similar macroscopic properties such as porosity particle size and connectivity, which could converge to statistically consistent porosity-permeability relationships. This way it could be possible to obtain reliable porosity-permeability and porosity-diffusivity relationships for continuum scale simulations, in a parametric form as function of porosity, Pe, Da and Re numbers based on microscopic pore scale simulations.

OUTLOOK: FUTURE NEEDS FOR THE MODEL DEVELOPMENT

With a set of case studies we could demonstrate that evolution of chemical and transport properties of reacting system strongly depend on underlying pore network structure, spatial variations of solutes concentration and their gradients. Robust simulations of pore scale transport would need efficient algorithms for pore microstructure generation and 3D imaging (Blunt and others, 2013). Several promising pore structure generation approaches have been proposed and need to be further optimized for more effective use in 3D simulations (Mezedur and others, 2002; Raoof and others, 2013; Tyagi and others, 2013). Molecular simulations further reveal inhomogeneous distribution of ions near the surface of charged minerals. The observed concentration differences can be as high as several orders of magnitude compared to the bulk (see fig. 5). Numerous experimental and modeling evidence exist that the ions adsorbed onto the mineral surface remain partially mobile (Gimmi and Kosakowski, 2011). Thus inhomogeneous ion distribution and partial mobility of the ions need to be incorporated in the pore scale reactive transport simulations (Mohajeri and others, 2010; Rotenberg and others, 2010; Obliger and others, 2013).

Within the porous structure, the mineral dissolution and precipitation processes alter the pore-topology in a strongly non-linear way. We have shown with a simple example that small changes in the porosity due to precipitation can have a very strong effect in the permeability of the porous medium, depending on the concentration gradients and the nucleation mechanisms. This clarifies that for an evolving porous media, it is not possible to have a universal correlation that will describe for example the permeability evolution, based solely on parameters like the porosity and the reactive surface area (Kozeny-Carman type), especially in the case of strong gradients or large time scales. It is evident that the result will always depend on a larger number of parameters, like the transport regime (diffusion, slow-fast advection), the pore-size distribution, the heterogeneity, the surface charges, the connectivity of the pores and other microstructural characteristics. Solution to this cumbersome task would improve the predictions of the macroscopic codes. At the moment this seems to be possible only by combining multiscale geochemical modeling (virtual toolbox) with detailed experiments in controlled environments in order to decipher the underlying mechanisms. Novel promising computing techniques like machine learning, big data analytics and artificial intelligence can possibly reduce the computational cost and effort, and aid in obtaining the required understanding.

Most of reactive transport simulations are performed using rigid models for porous media. Precipitation and mineral replacement reaction with positive volume change will result in local crystallization stresses. These stresses can lead to mechanical deformations and even cracking in the media. Typical examples of such phenomena are alkali silicate reactions in concrete and salt crystallization induced cracking (Alnaggar and others, 2013; Serafeimidis and Anagnostou, 2014; Desarnaud and others, 2016). Crystallization induced mechanical cracking can potentially keep the clogging interfaces open. Future pore scale reactive transport simulation models will

need to address these phenomena as well, by incorporating the effect of mechanical stresses.

Finally, the development of pore scale simulation methods must go hand in hand with the experimental characterization of reactive transport processes. Even the most advanced simulation techniques need to be validated by experimental studies. Particularly promising in this context are the non-destructive reactive *in situ* transport experiments combined with X-ray and neutron imaging (Godinho and others, 2016; Menke and others, 2016).

ACKNOWLEDGMENTS

Authors acknowledge inspiring discussions with colleagues: R. Arvidson, E. Curti, D. Grolimund, C. Fischer, A. Lüttge, D. Passerone, Th. Gimmi, G. Kosakowski, D. Kulik, I. Kurganskaya and Ch. Labbez. Special thanks go to Professor Sepehrnoori for providing visualization of reservoir simulations. The authors acknowledge partial financial support by Nagra, Swiss National Science Foundations (Grants ID: 130419, 156412, 165548, 172618) and access to the Swiss Centre of Scientific Computing (CSCS-Lugano).

APPENDIX 1

Molecular dynamics simulations of kaolinite, pyrophyllite and montmorillonite-water interfaces we performed with CLAYFF (Cygan and others, 2004) interaction parameters using LAMMPS simulation package(site: http://lammps.sandia.gov/) at constant pressure (P = 1 bar) and temperature (T=298 K). Flexible SPC/E model was applied for water. The integration of the equation of motion was performed with 0.5 fs time step. The production runs spans 10 ns long trajectory followed by 1 ns equilibration. 6000 snapshots were stored for data analysis. Average lattice parameters of the simulated system are summarized in table A1. The simulation box contained 2 layers of clay minerals, 280 water molecules and 5 NaCl units, resembling a 1 M NaCl solution. Six isomorphous substitution of Mg for Al were in each octahedral layer. Accordingly slit pore of the montmorillonite contained 6 Na ions in addition to the background electrolyte.

TABLE A1

	Chemical Composition	Solution	Supercell parameters [Å]
Pyrophyllite	$32 \times [Al_2Si_4O_{10}(OH)_2]$	280 H_2O × 5 NaCl	20.75 ×18.00 × 42.15
Montmorillonite	$4 \times [Na_3(Mg_3Al_{13})Si_{32}O_{80}(OH_{16}]$	280 H_2O × 5 NaCl	20.72 × 17.97 × 41.56
Kaolinite	$32 \times [Al_2Si_2O_5(OH)_4]$	280 H_2O × 5 NaCl	20.77 × 17.85 × 37.70

APPENDIX 2

The simulation method and the details of the system setups can be found in (Churakov and others, 2014). The surface of tobermorite was assumed to be built by pairs of Si-tetrahedra (all bridging tetrahedra removed). The GCMC model of tobermorite surface was represented by a planar interface with point >OH groups. The reactive surface sites were represented by aligned pairs (2.6 Å apart), representing silicate chains according to the structural position of apical oxygen sites of bridging tetrahedra. The pair centers along the chain are separated by 4.9 Å. The distance between chains was 5.65 Å resulting in the site density 4.82 sites nm^{-2}. The mineral surface is represented by OH groups according to the mineral structure with intrinsic pKa constants 6.15 and 8.85 as obtained by *ab initio* molecular dynamics simulations (Churakov and others, 2014). The dimensions of simulation box was larger then $170 \times 170 \times 170$ $Å^3$. Ions are represented by charged spheres with the radius equal to 2 Å. The solvent is replaced by a dielectric continuum with relative permittivity equal to 78. The surface sites titrate according to the imposed pH and the electrostatic interaction with ions and the surface sites in the system.

REFERENCES

Alnaggar, M., Cusatis, G., and Di Luzio, G., 2013, Lattice Discrete Particle Modeling (LDPM) of Alkali Silica Reaction (ASR) deterioration of concrete structures: Cement & Concrete Composites, v. 41, p. 45–59, https://doi.org/10.1016/j.cemconcomp.2013.04.015

Arvidson, R. S., Collier, M., Davis, K. J., Vinson, M. D., Amonette, J. E., and Lüttge, A., 2006, Magnesium inhibition of calcite dissolution kinetics: Geochimica et Cosmochimica Acta, v. 70, n. 3, p. 583–594, https://doi.org/10.1016/j.gca.2005.10.005

Battiato, I., and Tartakovsky, D. M., 2011, Applicability regimes for macroscopic models of reactive transport in porous media: Journal of Contaminant Hydrology, v. 120–121, p. 18–26, https://doi.org/10.1016/j.jconhyd.2010.05.005

Blum, A., and Lasaga, A., 1988, Role of surface speciation in the low-temperature dissolution of minerals: Nature, v. 331, p. 431–433, https://doi.org/10.1038/331431a0

Blunt, M. J., 2001, Flow in porous media - pore-network models and multiphase flow: Current Opinion in Colloid & Interface Science, v. 6, n. 3, p. 197–207, https://doi.org/10.1016/S1359-0294(01)00084-X

Blunt, M. J., Bijeljic, B., Dong, H., Gharbi, O., Iglauer, S., Mostaghimi, P., Paluszny, A., and Pentland, C., 2013, Pore-scale imaging and modeling: Advances in Water Resources, v. 51, p. 197–216, https://doi.org/10.1016/j.advwatres.2012.03.003

Botan, A., Rotenberg, B., Marry, V., Turq, P., and Noetinger, B., 2011, Hydrodynamics in Clay Nanopores: Journal of Physical Chemistry C, v. 115, n. 32, p. 16109–16115, https://doi.org/10.1021/jp204772c

Brantley, S. L., Kubicki, J. D., and White, A. F., editors, 2007, Kinetics of water-rock interaction: New York, Springer, 833 p.

Chatelin, R., and Poncet, P., 2013, A Hybrid Grid-Particle Method for Moving Bodies in 3D Stokes Flow with Variable Viscosity: Siam Journal on Scientific Computing, v. 35, n. 4, p. B925–B949, https://doi.org/10.1137/120892921

Cheng, J., and Sprik, M., 2014, The electric double layer at a rutile TiO2 water interface modelled using density functional theory based molecular dynamics simulation: Journal of Physics-Condensed Matter, v. 26, n. 24, https://doi.org/10.1088/0953-8984/26/24/244108

Churakov, S. V., 2013, Mobility of Na and Cs on Montmorillonite Surface under Partially Saturated Conditions: Environmental Science & Technology, v. 47, n. 17, p. 9816–9823, https://doi.org/10.1021/es401530n

Churakov, S. V., and Daehn, R., 2012, Zinc Adsorption on Clays Inferred from Atomistic Simulations and EXAFS Spectroscopy: Environmental Science & Technology, v. 46, n. 11, p. 5713–5719, https://doi.org/10.1021/es204423k

Churakov, S. V., and Gimmi, T., 2011, Up-scaling of molecular diffusion coefficients in clays: A two-step approach: The Journal of Physical Chemistry C, v. 115, n. 14, p. 6703–6714, https://doi.org/10.1021/jp112325n

Churakov, S. V., and Labbez, C., 2017, Thermodynamics and Molecular Mechanism of Al Incorporation in Calcium Silicate Hydrates: The Journal of Physical Chemistry C, v. 121, n. 8, p. 4412–4419, https://doi.org/10.1021/acs.jpcc.6b12850

Churakov, S. V., Iannuzzi, M., and Parrinello, M., 2004, *Ab Initio* study of dehydroxylation-carbonation reaction on brucite surface: The Journal of Physical Chemistry B, v. 108, n. 31, p. 11567–11574, https://doi.org/10.1021/jp037935x

Churakov, S. V., Labbez, C., Pegado, L., and Sulpizi, M., 2014, Intrinsic acidity of surface sites in calcium-silicate-hydrates and its implication to their electrokinetic properties: The Journal of Physical Chemistry C, v. 118, p. 11752–11762, https://doi.org/10.1021/jp502514a

De La Pierre, M., Raiteri, P., and Gale, J. D., 2016, Structure and Dynamics of Water at Step Edges on the Calcite {101–4} Surface: Crystal Growth & Design, v. 16, n. 10, p. 5907–5914, https://doi.org/10.1021/acs.cgd.6b00957

De La Pierre, M., Raiteri, P., Stack, A. G., and Gale, J. D., 2017, Uncovering the Atomistic Mechanism for Calcite Step Growth: Angewandte Chemie-International Edition, v. 56, n. 29, p. 8464–8467, https://doi.org/10.1002/anie.201701701

Desarnaud, J., Bonn, D., and Shahidzadeh, N., 2016, The Pressure induced by salt crystallization in confinement: Scientific Reports, v. 6, p. 8, https://doi.org/10.1038/srep30856

Fischer, C., and Lüttge, A., 2017, Beyond the conventional understanding of water-rock reactivity: Earth and Planetary Science Letters, v. 457, p. 100–105, https://doi.org/10.1016/j.epsl.2016.10.019

Fischer, C., Kurganskaya, I., Schäfer, T., and Lüttge, A., 2014, Variability of crystal surface reactivity: What do we know?: Applied Geochemistry, v. 43, p. 132–157, https://doi.org/10.1016/j.apgeochem.2014.02.002

Fischer, C., Finkeldei, S., Brandt, F., Bosbach, D., and Lüttge, A., 2015, Direct measurement of surface dissolution rates in potential nuclear waste forms: The example of pyrochlore: ACS Applied Materials & Interfaces, v. 7, n. 32, p. 17857–17865, https://doi.org/10.1021/acsami.5b04281

Fredd, C. N., and Fogler, H. S., 1998, Influence of transport and reaction on wormhole formation in porous media: Aiche Journal, v. 44, n. 9, p. 1933–1949, https://doi.org/10.1002/aic.690440902

Freij, S. J., Godelitsas, A., and Putnis, A., 2005, Crystal growth and dissolution processes at the calcite-water interface in the presence of zinc ions: Journal of Crystal Growth, v. 273, n. 3–4, p. 535–545, https://doi.org/10.1016/j.jcrysgro.2004.09.026

Frisch, U., Hasslacher, B., and Pomeau, Y., 1986, Lattice-Gas Automata for the Navier-Stokes Equation: Physical Review Letters, v. 56, p. 1505–1508, https://doi.org/10.1103/PhysRevLett.56.1505

Gimmi, T., and Kosakowski, G., 2011, How Mobile Are Sorbed Cations in Clays and Clay Rocks?: Environmental Science & Technology, v. 45, n. 4, p. 1443–1449, https://doi.org/10.1021/es1027794

Godinho, J. R. A., Gerke, K. M., Stack, A. G., and Lee, P. D., 2016, The dynamic nature of crystal growth in pores: Scientific Reports, v. 6, p. 7, https://doi.org/10.1038/srep33086

Golfier, F., Zarcone, C., Bazin, B., Lenormand, R., Lasseux, D., and Quintard, M., 2002, On the ability of a Darcy-scale model to capture wormhole formation during the dissolution of a porous medium: Journal of Fluid Mechanics, v. 457, p. 213–254, https://doi.org/10.1017/S0022112002007735

Hiemstra, T., and Van Riemsdijk, W. H., 1996, A Surface Structural Approach to Ion Adsorption: The Charge

Distribution (CD) Model: Journal of Colloid and Intarface Science, v. 179, n. 2, p. 488–508, https://doi.org/10.1006/jcis.1996.0242
Hofmann, S., Voitchovsky, K., Spijker, P., Schmidt, M., and Stumpf, T., 2016, Visualising the molecular alteration of the calcite (104) - water interface by sodium nitrate: Scientific Reports, v. 6, https://doi.org/10.1038/srep21576
Huber, C., Shafei, B., and Parmigiani, A., 2014, A new pore-scale model for linear and non-linear heterogeneous dissolution and precipitation: Geochimica et Cosmochimica Acta, v. 124, p. 109–130, https://doi.org/10.1016/j.gca.2013.09.003
Hughes, R. G., and Blunt, M. J., 2001, Network modeling of multiphase flow in fractures: Advances in Water Resources, v. 24, n. 3–4, p. 409–421, https://doi.org/10.1016/S0309-1708(00)00064-6
Kalinichev, A. G., and Kirkpatrick, R. J., 2002, Molecular dynamics modeling of chloride binding to the surfaces of calcium hydroxide, hydrated calcium aluminate, and calcium silicate phases: Chemistry of Materials, v. 14, n. 8, p. 3539–3549, https://doi.org/10.1021/cm0107070
Kang, J., Prasianakis, N. I., and Mantzaras, J., 2014, Thermal multicomponent lattice Boltzmann model for catalytic reactive flows: Physical Review E, v. 89, n. 6, 063310, https://doi.org/10.1103/PhysRevE.89.063310
Kang, Q., Zhang, D. X., Chen, S. Y., and He, X. Y., 2002, Lattice Boltzmann simulation of chemical dissolution in porous media: Physical Review E, v. 65, https://doi.org/10.1103/PhysRevE.65.036318
Kang, Q., Lichtner, P. C., and Zhang, D. X., 2006, Lattice Boltzmann pore-scale model for multicomponent reactive transport in porous media: Journal of Geophysical Research-Solid Earth, v. 111, n. B5, https://doi.org/10.1029/2005JB003951
Kang, Q., Chen, L., Valocchi, A. J., and Viswanathan, H. S., 2014, Pore-scale study of dissolution-induced changes in permeability and porosity of porous media: Journal of Hydrology, v. 517, p. 1049–1055, https://doi.org/10.1016/j.jhydrol.2014.06.045
Kashchiev, D., and van Rosmalen, G. M., 2003, Review: Nucleation in solutions revisited: Crystal Research and Technology, v. 38, n. 7–8, p. 555–574, https://doi.org/10.1002/crat.200310070
Kremleva, A., Martorell, B., Krueger, S., and Roesch, N., 2012, Uranyl adsorption on solvated edge surfaces of pyrophyllite: A DFT model study: Physical Chemistry Chemical Physics, v. 14, n. 16, p. 5815–5823, https://doi.org/10.1039/c2cp23886a
Kulik, D. A., 2009, Thermodynamic Concepts in Modeling Sorption at the Mineral-Water Interface, *in* Oelkers, E. H., and Schott, J., editors, Thermodynamics and Kinetics of Water-Rock Interaction: Reviews in Mineralogy & Geochemistry, p. 125–180, https://doi.org/10.2138/rmg.2009.70.4
Kurganskaya, I., and Lüttge, A., 2013a, A comprehensive stochastic model of phyllosilicate dissolution: Structure and kinematics of etch pits formed on muscovite basal face: Geochimica et Cosmochimica Acta, v. 120, p. 545–560, https://doi.org/10.1016/j.gca.2013.06.038
——— 2013b, Kinetic Monte Carlo Simulations of Silicate Dissolution: Model Complexity and Parametrization: The Journal of Physical Chemistry C, v. 117, n. 47, p. 24894–24906, https://doi.org/10.1021/jp408845m
——— 2016, Kinetic Monte Carlo Approach To Study Carbonate Dissolution: The Journal of Physical Chemistry C, v. 120, n. 12, p. 6482–6492, https://doi.org/10.1021/acs.jpcc.5b10995
Labbez, C., and Joensson, B., 2007, A new Monte Carlo method for the titration of molecules and minerals, *in* Kagstrom, B., Elmroth, E., Dongarra, J., and Wasniewski, J., editors, Applied Parallel Computing, State of the Art in Scientific Computing: Lecture Notes in Computer Science: Berlin, Springer, v. 4699, p. 66–72, https://doi.org/10.1007/978-3-540-75755-9_8
Labbez, C., Pochard, I., Jönsson, B., and Nonat, A., 2011, C-S-H/solution interface: Experimental and Monte Carlo studies: Cement and Concrete Research, v. 41, n. 2, p. 161–168, https://doi.org/10.1016/j.cemconres.2010.10.002
Lasaga, A. C., and Blum, A. E., 1986, Surface-chemistry, etch pits and mineral-water reactions.: Geochimica et Cosmochimica Acta, v. 50, n. 10, p. 2363–2379, https://doi.org/10.1016/0016-7037(86)90088-8
Lasaga, A. C., and Gibbs, G. V., 1990, *Ab-initio* quantum mechnical calculations of water-rock interactions: Adsorption and hydrolysis reactions: American Journal of Science, v. 290, n. 3, p. 263–295, https://doi.org/10.2475/ajs.290.3.263
Lasaga, A. C., and Luttge, A., 2001, Variation of crystal dissolution rate based on a dissolution stepwave model: Science, v. 291, n. 5512, p. 2400–2404, https://doi.org/10.1126/science.1058173
——— 2003, A model for crystal dissolution: European Journal of Mineralogy, v. 15, n. 4, p. 603–615, https://doi.org/10.1127/0935-1221/2003/0015-0603
——— 2004, Mineralogical approaches to fundamental crystal dissolution kinetics: American Mineralogist, v. 89, n. 4, p. 527–540, https://doi.org/10.2138/am-2004-0407
Lea, A. S., Amonette, J. E., Baer, D. R., Liang, Y., and Colton, N. G., 2001, Microscopic effects of carbonate, manganese, and strontium ions on calcite dissolution: Geochimica et Cosmochimica Acta, v. 65, n. 3, p. 369–379, https://doi.org/10.1016/S0016-7037(00)00531-7
Liu, X., Lu, X., Wang, R., Meijer, E. J., and Zhou, H., 2011, Acidities of confined water in interlayer space of clay minerals: Geochimica et Cosmochimica Acta, v. 75, n. 17, p. 4978–4986, https://doi.org/10.1016/j.gca.2011.06.011
Liu, X., Meijer, E. J., Lu, X., and Wang, R., 2012, First-principles molecular dynamics insight into Fe^{2+} complexes adsorbed on edge surfaces of clay minerals: Clays and Clay Minerals, v. 60, n. 4, p. 341–347, https://doi.org/10.1346/CCMN.2012.0600401
Lüttge, A., Arvidson, R. S., and Fischer, C., 2013, A Stochastic Treatment of Crystal Dissolution Kinetics: Elements, v. 9, n. 3, p. 183–188, https://doi.org/10.2113/gselements.9.3.183
Lutzenkirchen, J., 2002, Surface complexation models of adsorption: Encyclopedia of Surface and Colloid Science, p. 5028–5046.

Lyklema, J., 1995, Fundamentals of Interface and Colloid Science v. 2: London, England, Academic Press, 59 p.

Marry, V., Rotenberg, B., and Turq, P., 2008, Structure and dynamics of water at a clay surface from molecular dynamics simulation: Physical Chemistry Chemical Physics, v. 10, n. 32, p. 4802–4813, https://doi.org/10.1039/b807288d

Marty, N. C. M., Tournassat, C., Burnol, A., Giffaut, E., and Gaucher, E. C., 2009, Influence of reaction kinetics and mesh refinement on the numerical modeling of concrete/clay interactions: Journal of Hydrology, v. 364, n. 1–2, p. 58–72, https://doi.org/10.1016/j.jhydrol.2008.10.013

McGrail, B. P., Schaef, H. T., Spane, F. A., Cliff, J. B., Qafoku, O., Horner, J. A., Thompson, C. J., Owen, A. T., and Sullivan, C. E., 2017, Field Validation of Supercritical CO_2 Reactivity with Basalts: Environmental Science & Technology Letters, v. 4, n. 1, p. 6–10, https://doi.org/10.1021/acs.estlett.6b00387

Menke, H. P., Andrew, M. G., Blunt, M. J., and Bijeljic, B., 2016, Reservoir condition imaging of reactive transport in heterogeneous carbonates using fast synchrotron tomography – Effect of initial pore structure and flow conditions: Chemical Geology, v. 428, p. 15–26, https://doi.org/10.1016/j.chemgeo.2016.02.030

Mezedur, M. M., Kaviany, M., and Moore, W., 2002, Effect of pore structure, randomness sand size on effective mass diffusivity: AIChE Journal, v. 48, n. 1, p. 15–24, https://doi.org/10.1002/aic.690480104

Mohajeri, A., Narsilio, G. A., Pivonka, P., and Smith, D. W., 2010, Numerical estimation of effective diffusion coefficients for charged porous materials based on micro-scale analyses: Computers and Geotechnics, v. 37, n. 3, p. 280–287, https://doi.org/10.1016/j.compgeo.2009.10.004

Molins, S., Trebotich, D., Steefel, C. I., and Shen, C. P., 2012, An investigation of the effect of pore scale flow on average geochemical reaction rates using direct numerical simulation: Water Resources Research, v. 48, n. 3, https://doi.org/10.1029/2011WR011404

Moore, G. E., 1998, Cramming more components onto integrated circuits (Reprinted from Electronics, p. 114–117, April 19, 1965): Proceedings of the IEEE, v. 86, n. 1, p. 82–85, https://doi.org/10.1109/JPROC.1998.658762

Morse, J. W., Arvidson, R. S., and Lüttge, A., 2007, Calcium carbonate formation and dissolution: Chemical Reviews, v. 107, n. 2, p. 342–381, https://doi.org/10.1021/cr050358j

Mucci, A., and Morse, J. W., 1983, The incorporation of $Mg^{2+}$and Sr^{2+} into calcite overgrowths: Influences of growth rate and solution composition: Geochimica et Cosmochimica Acta, v. 47, n. 2, p. 217–233, https://doi.org/10.1016/0016-7037(83)90135-7

Obliger, A., Duvail, M., Jardat, M., Coelho, D., Békri, S., and Rotenberg, B., 2013, Numerical homogenization of electrokinetic equations in porous media using lattice-Boltzmann simulations: Physical Review E, v. 88, n. 1, https://doi.org/10.1103/PhysRevE.88.013019

Oelkers, E. H., Golubev, S. V., Chairat, C., Pokrovsky, O. S., and Schott, J., 2009, The surface chemistry of multi-oxide silicates: Geochimica et Cosmochimica Acta, v. 73, n. 16, p. 4617–4634, https://doi.org/10.1016/j.gca.2009.05.028

Parmigiani, A., Huber, C., Bachmann, O., and Chopard, B., 2011, Pore-scale mass and reactant transport in multiphase porous media flows: Journal of Fluid Mechanics, v. 686, p. 40–76, https://doi.org/10.1017/jfm.2011.268

Pokrovsky, O. S., Golubev, S. V., and Schott, J., 2005, Dissolution kinetics of calcite, dolomite and magnesite at 25 °C and 0 to 50 atm pCO_2: Chemical Geology, v. 217, n. 3–4, p. 239–255, https://doi.org/10.1016/j.chemgeo.2004.12.012

Pokrovsky, O. S., Golubev, S. V., Schott, J., and Castillo, A., 2009, Calcite, dolomite and magnesite dissolution kinetics in aqueous solutions at acid to circumneutral pH, 25 to 150 °C and 1 to 55 atm pCO_2: New constraints on CO_2 sequestration in sedimentary basins: Chemical Geology, v. 265, n. 1–2, p. 20–32, https://doi.org/10.1016/j.chemgeo.2009.01.013

Poonoosamy, J., Kosakowski, G., Van Loon, L. R., and Mäder, U., 2015, Dissolution–precipitation processes in tank experiments for testing numerical models for reactive transport calculations: Experiments and modeling: Journal of Contaminant Hydrology, v. 177–178, p. 1–17, https://doi.org/10.1016/j.jconhyd.2015.02.007

Poonoosamy, J., Curti, E., Kosakowski, G., Grolimund, D., Van Loon, L. R., and Mader, U., 2016, Barite precipitation following celestite dissolution in a porous medium: A SEM/BSE and μ-XRD/XRF study: Geochimica et Cosmochimica Acta, v. 182, p. 131–144, https://doi.org/10.1016/j.gca.2016.03.011

Prasianakis, N. I., Karlin, I. V., Mantzaras, J., and Boulouchos, K. B., 2009, Lattice Boltzmann method with restored Galilean invariance: Physical Review E, v. 79, 066702, https://doi.org/10.1103/PhysRevE.79.066702

Prasianakis, N. I., Rosén, T., Kang, J., Eller, J., Mantzaras, J., and Buchi, F. N., 2013, Simulation of 3D Porous Media Flows with Application to Polymer Electrolyte Fuel Cells: Communications in Computational Physics, v. 13, n. 3, p. 851–866, https://doi.org/10.4208/cicp.341011.310112s

Prasianakis, N. I., Curti, E., Kosakowski, G., Poonoosamy, J., and Churakov, S. V., 2017, Deciphering pore-level precipitation mechanisms: Scientific Reports, v. 7, p. 13765, https://doi.org/10.1038/s41598-017-14142-0

Prasianakis, N. I., Gatschet, M., Abbasi, A., and Churakov, S. V., 2018, Upscaling strategies of porosity-permeability correlations in reacting environments from pore-scale simulations.: Geofluids, p. 9260603–8, https://doi.org/10.1155/2018/9260603

Prieto, M., 2014, Nucleation and supersaturation in porous media (revisited): Mineralogical Magazine, v. 78, n. 6, p. 1437–1447, https://doi.org/10.1180/minmag.2014.078.6.11

Putnis, A., 2015, Transient Porosity Resulting from Fluid-Mineral Interaction and its Consequences, *in* Steefel, C. I., Emmanuel, S., and Anovitz, L. M., editors, Pore-Scale Geochemical Processes: Reviews in Mineralogy & Geochemistry, p. 1–23, https://doi.org/10.1515/9781501502071-001

Putnis, C. V., and Mezger, K., 2004, A mechanism of mineral replacement: Isotope tracing in the model

system KCl-KBr-H_2O: Geochimica et Cosmochimica Acta, v. 68, n. 13, p. 2839–2848, https://doi.org/10.1016/j.gca.2003.12.009
Putnis, C. V., and Ruiz-Agudo, E., 2013, The Mineral–Water Interface: Where Minerals React with the Environment: Elements, v. 9, n. 3, p. 177–182, https://doi.org/10.2113/gselements.9.3.177
Qian, Y. H., D'Dhumieres, D., and Lallemand, P., 1992, Lattice BGK Models for Navier-Stokes Equation: Europhysics Letters, v. 17, n. 6, p. 479–484, https://doi.org/10.1209/0295-5075/17/6/001
Raoof, A., and Hassanizadeh, S. M., 2010, A New Method for Generating Pore-Network Models of Porous Media: Transport in Porous Media, v. 81, n. 3, p. 391–407, https://doi.org/10.1007/s11242-009-9412-3
Raoof, A., Nick, H. M., Hassanizadeh, S. M., and Spiers, C. J., 2013, PoreFlow: A complex pore-network model for simulation of reactive transport in variably saturated porous media: Computers & Geosciences, v. 61, p. 160–174, https://doi.org/10.1016/j.cageo.2013.08.005
Revil, A., and Cathles, L. M., III, 1999, Permeability of shaly sands: Water Resources Research, v. 35, n. 3, p. 651–662, https://doi.org/10.1029/98WR02700
Rosen, T., Eller, J., Kang, J., Prasianakis, N. I., Mantzaras, J., and Büchi, F. N., 2012, Saturation Dependent Effective Transport Properties of PEFC Gas Diffusion Layers: Journal of the Electrochemical Society, v. 159, n. 9, p. F536–F544, https://doi.org/10.1149/2.005209jes
Rotenberg, B., Marry, V., Dufrêche, J.-F., Malikova, N., Giffaut, E., and Turq, P., 2007a, Modeling water and ion diffusion in clays: A multiscale approach: Comptes Rendus Chimie, v. 10, n. 10–11, p. 1108–1116, https://doi.org/10.1016/j.crci.2007.02.009
Rotenberg, B., Marry, V., Vuilleumier, R., Malikova, N., Simon, C., and Turq, P., 2007b, Water and ions in clays: Unraveling the interlayer/micropore exchange using molecular dynamics.: Geochimica et Cosmochimica Acta, v. 71, n. 21, p. 5089–5101, https://doi.org/10.1016/j.gca.2007.08.018
Rotenberg, B., Pagonabarraga, I., and Frenkel, D., 2010, Coarse-grained simulations of charge, current and flow in heterogeneous media: Faraday Discussions, v. 144, p. 223–243, https://doi.org/10.1039/B901553A
Ruiz-Agudo, E., Putnis, C. V., and Putnis, A., 2014, Coupled dissolution and precipitation at mineral-fluid interfaces: Chemical Geology, v. 383, p. 132–146, https://doi.org/10.1016/j.chemgeo.2014.06.007
Safi, M. A., Prasianakis, N., and Turek, S., 2017a, Benchmark computations for 3D two-phase flows: A coupled lattice Boltzmann-level set study: Computers & Mathematics with Applications, v. 73, n. 3, p. 520–536, https://doi.org/10.1016/j.camwa.2016.12.014
Safi, M. A., Prasianakis, N. I., Mantzaras, J., Lamibrac, A., and Buchi, F. N., 2017b, Experimental and pore-level numerical investigation of water evaporation in gas diffusion layers of polymer electrolyte fuel cells: International Journal of Heat and Mass Transfer, v. 115, Part A, p. 238–249, https://doi.org/10.1016/j.ijheatmasstransfer.2017.07.050
Sahai, N., and Sverjensky, D. A., 1997a, Evaluation of internally consistent parameters for the triple-layer model by the systematic analysis of oxide surface titration data.: Geochimica et Cosmochimica Acta, v. 61, n. 14, p. 2801–2826, https://doi.org/10.1016/S0016-7037(97)00128-2
——— 1997b, Solvation and electrostatic model for specific electrolyte adsorption: Geochimica et Cosmochimica Acta, v. 61, n. 14, p. 2827–2848, https://doi.org/10.1016/S0016-7037(97)00127-0
Serafeimidis, K., and Anagnostou, G., 2014, On the crystallisation pressure of gypsum: Environmental Earth Sciences, v. 72, n. 12, p. 4985–4994, https://doi.org/10.1007/s12665-014-3366-7
Soulaine, C., and Tchelepi, H. A., 2016, Micro-continuum Approach for Pore-Scale Simulation of Subsurface Processes: Transport in Porous Media, v. 113, n. 3, p. 431–456, https://doi.org/10.1007/s11242-016-0701-3
Stack, A. G., and Kent, P. R. C., 2015, Geochemical reaction mechanism discovery from molecular simulation: Environmental Chemistry, v. 12, n. 1, p. 20–32, https://doi.org/10.1071/EN14045
Steefel, C. I., Appelo, C. A. J., Arora, B., Jacques, D., Kalbacher, T., Kolditz, O., Lagneau, V., Lichtner, P. C., Mayer, K. U., Meeussen, J. C. L., Molins, S., Moulton, D., Shao, H., Simunek, J., Spycher, N., Yabusaki, S. B., and Yeh, G. T., 2015a, Reactive transport codes for subsurface environmental simulation: Computational Geosciences, v. 19, n. 3, p. 445–478, https://doi.org/10.1007/s10596-014-9443-x
Steefel, C. I., Emmanuel, S., and Anovitz, L. M., editors, 2015b, Pore-Scale Geochemical Processes: Reviews in Mineralogy & Geochemistry, v. 80, 491 p.
Succi, S., 2001, The Lattice Boltzmann Equation for fluid dynamics and beyond: Numerical mathematics and scientific computation: Oxford, England, Clarendon Press, 288 p.
Succi, S., Foti, E., and Higuera, F., 1989, Three-Dimensional Flows in Complex Geometries with the Lattice Boltzmann Method: Europhysics Letters, v. 10, n. 5, p. 433–438, https://doi.org/10.1209/0295-5075/10/5/008
Sverjensky, D. A., 2001, Interpretation and prediction of triple-layer model capacitances and the structure of the oxide–electrolyte–water interface: Geochimica et Cosmochimica Acta, v. 65, n. 21, p. 3643–3655, https://doi.org/10.1016/S0016-7037(01)00709-8
——— 2005, Prediction of surface charge on oxides in salt solutions: Revisions for 1 : 1 (M^+L^-) electrolytes: Geochimica et Cosmochimica Acta, v. 69, n. 2, p. 225–257, https://doi.org/10.1016/j.gca.2004.05.040
——— 2006, Prediction of the speciation of alkaline earths adsorbed on mineral surfaces in salt solutions: Geochimica et Cosmochimica Acta, v. 70, n. 10, p. 2427–2453, https://doi.org/10.1016/j.gca.2006.01.006
Szymczak, P., and Ladd, A. J. C., 2009, Wormhole formation in dissolving fractures: Journal of Geophysical Research-Solid Earth, v. 114, n. B6, https://doi.org/10.1029/2008JB006122
Tartakovsky, A. M., Meakin, P., Scheibe, T. D., and Wood, B. D., 2007, A smoothed particle hydrodynamics model for reactive transport and mineral precipitation in porous and fractured porous media: Water Resources Research, v. 43, n. 5, https://doi.org/10.1029/2005WR004770
Teng, H. H., 2004, Controls by saturation state on etch pit formation during calcite dissolution: Geochimica et Cosmochimica Acta, v. 68, n. 2, p. 253–262, https://doi.org/10.1016/S0016-7037(03)00423-X
Teng, H. H., Dove, P. M., Orme, C. A., and De Yoreo, J. J., 1998, Thermodynamics of calcite growth: Baseline

for understanding biomineral formation: Science, v. 282, n. 5389, p. 724–727, https://doi.org/10.1126/science.282.5389.724
Teng, H. H., Dove, P. M., and De Yoreo, J. J., 2000, Kinetics of calcite growth: Surface processes and relationships to macroscopic rate laws: Geochimica et Cosmochimica Acta, v. 64, n. 13, p. 2255–2266, https://doi.org/10.1016/S0016-7037(00)00341-0
Teppen, B. J., Rasmussen, K., Bertsch, P. M., Miller, D. M., and Schäfer, L., 1997, Molecular Dynamics Modeling of Clay Minerals. 1. Gibbsite, Kaolinite, Pyrophyllite, and Beidellite: The Journal of Physical Chemistry B, v. 101, n. 9, p. 1579–1587, https://doi.org/10.1021/jp961577z
Tesson, S., Salanne, M., Rotenberg, B., Tazi, S., and Marry, V., 2016, Classical Polarizable Force Field for Clays: Pyrophyllite and Talc: The Journal of Physical Chemistry C, v. 120, n. 7, p. 3749–3758, https://doi.org/10.1021/acs.jpcc.5b10181
Torrie, G. M., and Valleau, J. P., 1982, Electrical double layers. 4. Limitations of the Gouy-Chapman theory: The Journal of Physical Chemistry, v. 86, n. 16, p. 3251–3257, https://doi.org/10.1021/j100213a035
Tournassat, C., Chapron, Y., Leroy, P., Bizi, M., and Boulahya, F., 2009, Comparison of molecular dynamics simulations with triple layer and modified Gouy–Chapman models in a 0.1 M NaCl–montmorillonite system: Journal of Colloid and Interface Science, v. 339, n. 2, p. 533–541, https://doi.org/10.1016/j.jcis.2009.06.051
Tournassat, C., Grangeon, S., Leroy, P., and Giffaut, A. E., 2013, Modeling specific pH dependent sorption of divalent metals on montmorillonite surfaces. A review of pitfalls, recent achievements and current challenges: American Journal of Science, v. 313, n. 5, p. 395–451, https://doi.org/10.2475/05.2013.01
Trebotich, D., Adams, M. F., Molins, S., Steefel, C. I., and Shen, C. P., 2014, High-Resolution Simulation of Pore-Scale Reactive Transport Processes Associated with Carbon Sequestration: Computing in Science & Engineering, v. 16, n. 6, p. 22–31, https://doi.org/10.1109/MCSE.2014.77
Tyagi, M., Gimmi, T., and Churakov, S. V., 2013, Multi-scale micro-structure generation strategy for up-scaling transport in clays: Advances in Water Resources, v. 59, p. 181–195, https://doi.org/10.1016/j.advwatres.2013.06.002
Valleau, J. P., and Torrie, G. M., 1984, Electrical double-layers.V. Asymmetric ion wall interactions: The Journal of Chemical Physics, v. 81, n. 12, p. 6291–6295, https://doi.org/10.1063/1.447535
Van Loon, L. R., and Mibus, J., 2015, A modified version of Archie's law to estimate effective diffusion coefficients of radionuclides in argillaceous rocks and its application in safety analysis studies: Applied Geochemistry, v. 59, p. 85–94, https://doi.org/10.1016/j.apgeochem.2015.04.002
Vasconcelos, I. F., Bunker, B. A., and Cygan, R. T., 2007, Molecular Dynamics Modeling of Ion Adsorption to the Basal Surfaces of Kaolinite: The Journal of Physical Chemistry C, v. 111, n. 18, p. 6753–6762, https://doi.org/10.1021/jp065687+
Vinson, M. D., Arvidson, R. S., and Luttge, A., 2007, Kinetic inhibition of calcite (104) dissolution by aqueous manganese(II): Journal of Crystal Growth, v. 307, n. 1, p. 116–125, https://doi.org/10.1016/j.jcrysgro.2007.05.059
Wang, J., Kalinichev, A. G., and Kirkpatrick, R. J., 2004, Molecular modeling of water structure in nano-pores between brucite (001) surfaces: Geochimica et Cosmochimica Acta, v. 68, n. 16, p. 3351–3365, https://doi.org/10.1016/j.gca.2004.02.016
——— 2006, Effects of substrate structure and composition on the structure, dynamics, and energetics of water at mineral surfaces: A molecular dynamics modeling study: Geochimica et Cosmochimica Acta, v. 70, n. 3, p. 562–582, https://doi.org/10.1016/j.gca.2005.10.006
Wolthers, M., Charlet, L., and Van Cappellen, P., 2008, The surface chemistry of divalent metal carbonate minerals; a critical assessment of surface charge and potential data using the charge distribution multi-site ion complexation model: American Journal of Science, v. 308, n 8, p. 905–941, https://doi.org/10.2475/08.2008.02
Wolthers, M., Nehrke, G., Gustafsson, J. P., and Van Cappellen, P., 2012, Calcite growth kinetics: Modeling the effect of solution stoichiometry: Geochimica et Cosmochimica Acta, v. 77, p. 121–134, https://doi.org/10.1016/j.gca.2011.11.003
Xie, M. L., Mayer, K. U., Claret, F., Alt-Epping, P., Jacques, D., Steefel, C., Chiaberge, C., and Simunek, J., 2015, Implementation and evaluation of permeability-porosity and tortuosity-porosity relationships linked to mineral dissolution-precipitation: Computational Geosciences, v. 19, n. 3, p. 655–671, https://doi.org/10.1007/s10596-014-9458-3
Xu, J., Fan, C., and Teng, H. H., 2012, Calcite dissolution kinetics in view of Gibbs free energy, dislocation density, and pCO_2: Chemical Geology, v. 322–323, p. 11–18, https://doi.org/10.1016/j.chemgeo.2012.04.019
Xu, P., and Yu, B. M., 2008, Developing a new form of permeability and Kozeny-Carman constant for homogeneous porous media by means of fractal geometry: Advances in Water Resources, v. 31, n. 1, p. 74–81, https://doi.org/10.1016/j.advwatres.2007.06.003
Xiao, Y., and Lasaga, A. C., 1996, *Ab initio* quantum mechanical studies of the kinetics and mechanisms of quartz dissolution: OH- catalysis: Geochimica et Cosmochimica Acta, v. 60, n. 13, p. 2283–2295, https://doi.org/10.1016/0016-7037(96)00101-9
Zhang, C., Liu, X. D., Lu, X. C., He, M. J., Meijer, E. J., and Wang, R. C., 2017, Surface complexation of heavy metal cations on clay edges: Insights from first principles molecular dynamics simulation of Ni(II): Geochimica et Cosmochimica Acta, v. 203, p. 54–68, https://doi.org/10.1016/j.gca.2017.01.014
Zhang, C., Liu, X., Lu, X., and He, M., 2018, Complexation of heavy metal cations on clay edges at elevated temperatures: Chemical Geology, v. 479, p. 36–46, https://doi.org/10.1016/j.chemgeo.2017.12.027
Zhang, L., and Lüttge, A., 2007, Al,Si order in albite and its effect on albite dissolution processes: A Monte Carlo study: American Mineralogist, v. 92, 8–9, p. 1316–1324, https://doi.org/10.2138/am.2007.2471